

String-Averaging Incremental Subgradients for Constrained Convex Optimization with Applications to Reconstruction of Tomographic Images

Rafael Massambone de Oliveira¹, Elias Salomão Helou¹ and Eduardo Fontoura Costa¹

¹ University of São Paulo - Institute of Mathematics and Computer Sciences, Department of Applied Mathematics and Statistics, São Carlos-SP, CEP 13566-590, Brazil

E-mail: massambone@usp.br, elias@icmc.usp.br, efcosta@icmc.usp.br

Abstract. We present a method for non-smooth convex minimization which is based on subgradient directions and string-averaging techniques. In this approach, the set of available data is split into sequences (strings) and a given iterate is processed independently along each string, possibly in parallel, by an incremental subgradient method (ISM). The end-points of all strings are averaged to form the next iterate. The method is useful to solve sparse and large-scale non-smooth convex optimization problems, such as those arising in tomographic imaging. A convergence analysis is provided under realistic, standard conditions. Numerical tests are performed in a tomographic image reconstruction application, showing good performance for the convergence speed when measured as the decrease ratio of the objective function, in comparison to classical ISM.

Keywords: convex optimization, incremental algorithms, subgradient methods, projection methods, string-averaging algorithms.

1. Introduction

A fruitful approach to solve an inverse problem is to recast it as an optimization problem, leading to a more flexible formulation that can be handled with different techniques. The *reconstruction of tomographic images* is a classical example of a problem that has been explored by optimization methods, among which the well-known *incremental subgradient method* (ISM) [40, 42, 49], that is a variation of the *subgradient method* [27, 44, 47], features nice performance in terms of convergence speed. There are many papers that discuss incremental gradient/subgradient algorithms for convex/non-convex objective functions (smooth or not) with applications to several fields [7, 9, 10, 40, 48–53]. Some examples of applications to tomographic image reconstruction are found in [1, 12, 26, 34, 52]. In this paper, we consider a rather general optimization problem that can be addressed by ISM and is useful for tomographic reconstruction and other problems, including to find solutions for ill-conditioned and/or large-scale linear systems. This problem consists of determining:

$$\begin{aligned} & \mathbf{x} \in \arg \min f(\mathbf{x}) \\ \text{s.t. } & \mathbf{x} \in \mathbf{X} \subset \mathbb{R}^n, \end{aligned} \tag{1}$$

where:

- (i) $f(\mathbf{x}) := P \sum_{i=1}^m \xi_i f_i(\mathbf{x})$ in which $f_i : \mathbb{R}^n \rightarrow \mathbb{R}$ are convex (and possibly non-differentiable) functions;
- (ii) \mathbf{X} is a non-empty, convex and closed set;
- (iii) The set $\mathcal{I} = \{S_1, \dots, S_P\}$ is a *partition* of $\{1, \dots, m\}$, i.e., $S_\ell \cap S_j = \emptyset$ for any $\ell, j \in \{1, \dots, P\}$ with $\ell \neq j$ and $\bigcup_{\ell=1}^P S_\ell = \{1, \dots, m\}$;
- (iv) Given $w_\ell \in [0, 1]$ and $S_\ell \in \mathcal{I}$, $\ell = 1, \dots, P$, the weights ξ_i satisfy $\xi_i = w_\ell$ for all $i \in S_\ell$;
- (v) $\sum_{\ell=1}^P w_\ell = 1$.

Problem (1) with conditions (i)-(v) is reduced to the classical problem of minimizing $\sum_{i=1}^m f_i(\mathbf{x})$, s.t. $\mathbf{x} \in \mathbf{X}$, when $w_\ell = 1/P$ for all $\ell = 1, \dots, P$. The reason why we write the problem in this more complex way is twofold. On one hand, it is common to find problems in which a set of fixed weights are used to prioritize the contribution of some component functions. For instance, in the context of distributed networks, the component functions f_i (also called “agents”) can be affected by external conditions, network topology, traffic, etc., making possible that some sets of agents have a prevalent role on the network, which can be modeled by the weights (related to the corresponding subnets). On the other hand, the weights and the partition, which bring flexibility to the model and could possibly be explored aiming for instance at faster convergence, will fit naturally in our algorithmic framework.

We consider an approach that mixes ISM and *string-averaging algorithms* (SA algorithms). The general form of the SA algorithm was proposed initially in [13] and applied in solving *convex feasibility problems* (CFPs) with algorithms that use

projection methods [13, 14, 43]. Strings are created so that ISM (more generally, any ϵ -incremental subgradient method) can be processed in an independent form for each string (by step operators). Then, an average of string iterations is computed (combination operator), guiding the iterations towards the solution. To complete, approximate projections are used to maintain feasibility. We provide an analysis of convergence under reasonable assumptions, such as diminishing step-size rule and boundedness of the subgradients.

Some previous works in the literature have improved the understanding and practical efficiency of ISM by creating more general algorithmic structures, enabling a broader analysis of convergence and making them more robust and accurate [35, 40, 42, 50, 51]. We improve on those results by adding a string-averaging structure to the ISM that allows for an efficient parallel processing of a complete iteration which, consequently, can lead to fast convergence and suitable approximate solutions. Furthermore, the presented techniques present better smoothing properties in practice, which is good for imaging tasks. These features are desirable, especially when we seek to solve ill-conditioned/large scale problems. As mentioned at the beginning of this section, one of our goals is to obtain an efficient method for solving problems of reconstruction of tomographic images from incompletely sampled data.

Although our work is closely linked to ISM, it is important to mention other classes of methods that can be applied to convex optimization problems. Under reasonable assumptions, problem (1) can be solved using *proximal-type algorithms* (for a description of some of the main methods, see [24]). For instance, in [23] the authors propose a proximal decomposition method derived from the Douglas-Rachford algorithm and establish its weak convergence in Hilbert spaces. Some variants and generalizations of such methods can be found in [11, 17, 24, 25, 45]. The *bundle approach* [32] is often used for numerically solving non-differentiable convex optimization problems. Also, *first order accelerated techniques* [5, 6] form yet another family of popular techniques for convex optimization problem endowed with a certain separability property. The advantage of ISM over the aforementioned techniques lies in its lightweight iterations from the computational viewpoint, not even requiring sufficient decrease properties to be checked. Besides, ISM presents a fast practical convergence rate in the first iterations which enables this technique to achieve good reconstructions within a small amount of time even for the huge problem sizes that appear, for example, in tomography.

The *tomographic image reconstruction problem* consists in finding an image described by a function $\psi : \mathbb{R}^2 \rightarrow \mathbb{R}$ from samples of its *Radon Transform*, which can be recast into solving the linear system

$$R\mathbf{x} = \mathbf{b}, \tag{2}$$

where R is the discretization of the Radon Transform operator, \mathbf{b} contains the collected samples of the Radon Transform and the desired image is represented by the vector \mathbf{x} . We consider solving the problem (2), rewriting it as a minimization problem,

as in (1). Solving problem (2) from an optimization standpoint is not a new idea. In particular, [42] illustrates the application of some of the methods arising from a general framework to tomographic image reconstruction with a limited number of views. For the discretized problem (2), iterative methods such as ART (Algebraic Reconstruction Technique) [39], POCS (Projection Onto Convex Sets) [3, 22], and Cimmino [21] have been widely used in the past.

Tomographic image reconstruction is an inverse problem in the sense that the image ψ is to be obtained from the inversion of a linear compact operator, which is well known to be an ill-conditioned problem. While the specific case of Radon inversion has an analytical solution, that was published in 1917 by Johann Radon (for details see [38]), both such analytical techniques and the aforementioned iterative methods for linear systems of equations suffer from amplification of the statistical noise which, in practice, is always present in the right-hand side of (2). Therefore, methods designed to deal with noisy data have been developed, based on a maximum likelihood approach, among which EM (Expectation Maximization) [46, 54], OS-EM (Ordered Subsets Expectation Maximization) [34], RAMLA (Row-Action Maximum Likelihood Algorithm) [12], BSREM (Block Sequential Regularized Expectation Maximization) [26], DRAMA (Dynamic RAMLA) [41, 52], modified BSREM and relaxed OS-SPS (Ordered Subset-Separable Paraboloidal Surrogates) [1] are some of the best known in the literature. In [30], a variant of the EM algorithm was introduced, called *String-Averaging Expectation-Maximization (SAEM) algorithm*. The SAEM algorithm was used in problems of image reconstruction in *Single-Photon Emission Computerized Tomography (SPECT)* and showed good performance in simulated and real data studies. High-contrast images, with less noise and clearer object boundaries were reconstructed without incurring in more computation time. Besides the BSREM, DRAMA, modified BSREM and relaxed OS-SPS, that are relaxed algorithms for (penalized) maximum-likelihood image reconstruction in tomography, the method introduced in [28] considers an approach, based in OS-SPS, in which extra anatomical boundary information is used. Other methods that use penalized models can be found in [20, 29]. Proximal methods were used in [2] to reconstruct images obtained via *Cone Beam Computerized Tomography (CBCT)* and *Positron Emission Tomography (PET)*. In [20], the *Majorize-Minimize Memory Gradient algorithm* [18, 19] is studied and applied to imaging tasks.

The paper is organized as follows: Section 2 contains some preliminary theory involving incremental subgradient methods, optimality and feasibility operators and string-averaging algorithm; Section 3 discusses the proposed algorithm to solve (1), (i)-(v); Section 4 shows theoretical convergence results; in Section 5 numerical tests are performed with reconstruction of tomographic images. Final considerations are given in Section 6.

2. Preliminary theory

Throughout the text, we will use the following notations: bold-type notations e.g. \mathbf{x} , \mathbf{x}_i and \mathbf{x}_i^k are vectors whereas x is a number. We denote x_i as the i th coordinate of vector \mathbf{x} . Moreover,

$$\begin{aligned} \mathcal{P}_{\mathbf{X}}(\mathbf{x}) &:= \arg \min_{\mathbf{y} \in \mathbf{X}} \|\mathbf{y} - \mathbf{x}\|, \quad d_{\mathbf{X}}(\mathbf{x}) := \|\mathbf{x} - \mathcal{P}_{\mathbf{X}}(\mathbf{x})\|, \\ [x]_+ &:= \max\{0, x\}, \quad f^* = \inf_{\mathbf{x} \in \mathbf{X}} f(\mathbf{x}) \quad \text{and} \quad \mathbf{X}^* = \{\mathbf{x} \in \mathbf{X} \mid f(\mathbf{x}) = f^*\}, \end{aligned}$$

where we assume that $\mathbf{X}^* \neq \emptyset$.

One of the main methods for solving (1) is the *subgradient method*, whose extensive theory can be found in [8, 27, 32, 44, 47],

$$\mathbf{x}^{k+1} = \mathcal{P}_{\mathbf{X}} \left(\mathbf{x}^k - \lambda_k \sum_{i=1}^m \mathbf{g}_i^k \right), \quad \lambda_k > 0, \quad \mathbf{g}_i^k \in \partial f_i(\mathbf{x}^k), \quad (3)$$

where the *subdifferential* of $f : \mathbb{R}^n \rightarrow \mathbb{R}$ at \mathbf{x} (the set of all subgradients) can be defined by

$$\partial f(\mathbf{x}) := \{\mathbf{g} \mid f(\mathbf{x}) + \langle \mathbf{g}, \mathbf{z} - \mathbf{x} \rangle \leq f(\mathbf{z}), \forall \mathbf{z}\}. \quad (4)$$

A similar approach to (3), known as *incremental subgradient method*, was studied firstly by Kibardin in [37] and then analyzed by Solodov and Zavriev in [49], in which a complete iteration of the algorithm can be described as follows:

$$\begin{aligned} \mathbf{x}_0^k &= \mathbf{x}^k \\ \mathbf{x}_i^k &= \mathbf{x}_{i-1}^k - \lambda_k \mathbf{g}_i^k, \quad i = 1, \dots, m, \quad \mathbf{g}_i^k \in \partial f_i(\mathbf{x}_{i-1}^k) \\ \mathbf{x}^{k+1} &= \mathcal{P}_{\mathbf{X}}(\mathbf{x}_m^k). \end{aligned} \quad (5)$$

A variant of this algorithm that uses projection onto \mathbf{X} to compute the sub-iterations \mathbf{x}_i^k was analyzed in [40].

The method we propose in this paper for solving the problem given in (1), **(i)-(v)** has the following general form described in [42]:

$$\begin{aligned} \mathbf{x}^{k+1/2} &= \mathcal{O}_f(\lambda_k, \mathbf{x}^k); \\ \mathbf{x}^{k+1} &= \mathcal{V}_{\mathbf{X}}(\mathbf{x}^{k+1/2}). \end{aligned} \quad (6)$$

In the above equations, \mathcal{O}_f is called *optimality operator* and $\mathcal{V}_{\mathbf{X}}$ is the *feasibility operator*. This framework was created to handle quite general algorithms for convex optimization problems. The basic idea consists in dividing an iterate in two parts: an optimality step which tries to guide the iterate towards the minimizer of the objective function (but not necessarily in a descent direction), followed by the feasibility step that drives the iterate in the direction of feasibility.

Next we enunciate a result due to Helou and De Pierro (see [42, Theorem 2.5]), establishing convergence of the method (6) under some conditions. This result is the key for the convergence analysis of the algorithm we propose in section 3.

Theorem 2.1. *The sequence $\{\mathbf{x}^k\}$ generated by the method described in (6) converges in the sense that*

$$d_{\mathbf{X}^*}(\mathbf{x}^k) \rightarrow 0 \quad \text{and} \quad \lim_{k \rightarrow \infty} f(\mathbf{x}^k) = f^*,$$

if all of the following conditions hold:

Condition 1 (Properties of optimality operator). *For every $\mathbf{x} \in \mathbf{X}$ and for all sequence $\lambda_k \geq 0$, there exist $\alpha > 0$ and a sequence $\rho_k \geq 0$ such that the optimality operator \mathcal{O}_f satisfies for all $k \geq 0$*

$$\|\mathcal{O}_f(\lambda_k, \mathbf{x}^k) - \mathbf{x}\|^2 \leq \|\mathbf{x}^k - \mathbf{x}\|^2 - \alpha \lambda_k (f(\mathbf{x}^k) - f(\mathbf{x})) + \lambda_k \rho_k. \quad (7)$$

We further assume that the error term in the above inequality vanishes, i.e., $\rho_k \rightarrow 0$ and we consider a boundedness property for the optimality operator: there is $\gamma > 0$ such that

$$\|\mathbf{x}^k - \mathcal{O}_f(\lambda_k, \mathbf{x}^k)\| \leq \lambda_k \gamma. \quad (8)$$

Condition 2 (Property of feasibility operator). *For the feasibility operator $\mathcal{V}_{\mathbf{X}}$, we impose that for all $\delta > 0$, exists $\epsilon_\delta > 0$ such that, if $d_{\mathbf{X}}(\mathbf{x}^{k+1/2}) \geq \delta$ and $\mathbf{x} \in \mathbf{X}$ we have*

$$\|\mathcal{V}_{\mathbf{X}}(\mathbf{x}^{k+1/2}) - \mathbf{x}\|^2 \leq \|\mathbf{x}^{k+1/2} - \mathbf{x}\|^2 - \epsilon_\delta. \quad (9)$$

Moreover, for all $\mathbf{x} \in \mathbf{X}$, $\mathcal{V}_{\mathbf{X}}(\mathbf{x}) = \mathbf{x}$, i.e., \mathbf{x} is a fixed point of $\mathcal{V}_{\mathbf{X}}$.

Condition 3 (Diminishing step-size rule). *The sequence $\{\lambda_k\}$ satisfies*

$$\lambda_k \rightarrow 0^+, \quad \sum_{k=0}^{\infty} \lambda_k = \infty. \quad (10)$$

Condition 4. *The optimal set \mathbf{X}^* is bounded, $\{d_{\mathbf{X}}(\mathbf{x}^k)\}$ is bounded and*

$$[f(\mathcal{P}_{\mathbf{X}}(\mathbf{x}^k)) - f(\mathbf{x}^k)]_+ \rightarrow 0.$$

Remark 2.2. Regarding the requirement $[f(\mathcal{P}_{\mathbf{X}}(\mathbf{x}^k)) - f(\mathbf{x}^k)]_+ \rightarrow 0$, it holds if there is a bounded sequence $\{\mathbf{v}^k\}$ where $\mathbf{v}^k \in \partial f(\mathcal{P}_{\mathbf{X}}(\mathbf{x}^k))$ and $d_{\mathbf{X}}(\mathbf{x}^k) \rightarrow 0$. Indeed,

$$\langle \mathbf{v}^k, \mathbf{y} - \mathcal{P}_{\mathbf{X}}(\mathbf{x}^k) \rangle \leq f(\mathbf{y}) - f(\mathcal{P}_{\mathbf{X}}(\mathbf{x}^k)), \quad \forall \mathbf{y} \in \mathbb{R}^n.$$

By Cauchy-Schwarz inequality, we have $\|\mathbf{v}^k\| \|\mathcal{P}_{\mathbf{X}}(\mathbf{x}^k) - \mathbf{y}\| \geq [f(\mathcal{P}_{\mathbf{X}}(\mathbf{x}^k)) - f(\mathbf{y})]_+$. Taking $\mathbf{y} = \mathbf{x}^k$, then $d_{\mathbf{X}}(\mathbf{x}^k) \rightarrow 0$ ensures that $[f(\mathcal{P}_{\mathbf{X}}(\mathbf{x}^k)) - f(\mathbf{x}^k)]_+ \rightarrow 0$. Therefore, under this mild boundedness assumption on the subdifferentials $\partial f(\mathcal{P}_{\mathbf{X}}(\mathbf{x}^k))$, proving that $d_{\mathbf{X}}(\mathbf{x}^k) \rightarrow 0$ also ensures that $[f(\mathcal{P}_{\mathbf{X}}(\mathbf{x}^k)) - f(\mathbf{x}^k)]_+ \rightarrow 0$.

Concerning the assumption $d_{\mathbf{X}}(\mathbf{x}^k) \rightarrow 0$, Proposition 2.1 in [42] shows that it holds if $\{d_{\mathbf{X}}(\mathbf{x}^k)\}$ is bounded, $\lambda_k \rightarrow 0^+$, and Equation (8) plus Condition 2 hold. Since Condition 4 requires $\{d_{\mathbf{X}}(\mathbf{x}^k)\}$ to be bounded, then we have that $[f(\mathcal{P}_{\mathbf{X}}(\mathbf{x}^k)) - f(\mathbf{x}^k)]_+ \rightarrow 0$ just under the boundedness assumption on $\partial f(\mathcal{P}_{\mathbf{X}}(\mathbf{x}^k))$. Furthermore, Corollary 2.7 in [42] states that $d_{\mathbf{X}}(\mathbf{x}^k) \rightarrow 0$ if $\lambda_k \rightarrow 0^+$, Conditions 1 and 2 hold and there is f_l such that $f(\mathbf{x}^k) \geq f_l$ for all k . Basically, the hypotheses of this corollary allow to show that $\{d_{\mathbf{X}}(\mathbf{x}^k)\}$ is bounded and result follow by Proposition 2.1. This is the situation that occurs in our numerical experiment. Such remarks are important to show how the hypotheses of our main convergence result (see Corollary 4.5 in section 4) can be reasonable. \square

To state our algorithm in next section, we need to define the operators \mathcal{O}_f and \mathcal{V}_X . Below we present the last ingredient of our operator \mathcal{O}_f , the *String-Averaging (SA) algorithm*. Originally formulated in [13], SA algorithm consists of dividing an index set $I = \{1, 2, \dots, \eta\}$ into *strings* in the following manner

$$\Delta_\ell := \{i_1^\ell, i_2^\ell, \dots, i_{m(\ell)}^\ell\}, \quad (11)$$

where $m(\ell)$ represents the number of elements in the string Δ_ℓ and $\ell \in \{1, 2, \dots, N\}$. Let us consider \mathcal{X} and \mathcal{Y} as subsets of \mathbb{R}^n where $\mathcal{Y} \subseteq \mathcal{X}$. The basic idea behind the method consists in the sequential application of *step operators* $\mathcal{F}^{i_s^\ell} : \mathcal{X} \rightarrow \mathcal{Y}$, for each $s = 1, 2, \dots, m(\ell)$ over each string Δ_ℓ , producing N vectors $\mathbf{y}_\ell^k \in \mathcal{Y}$. Next, a *combination operator* $\mathcal{F} : \mathcal{Y}^N \rightarrow \mathcal{Y}$ mixes, usually by weighted average, all vectors \mathbf{y}_ℓ^k to obtain \mathbf{y}^{k+1} . We refer to the index s as the *step* and the index k as the *iteration*. Therefore, given $\mathbf{x}^0 \in \mathcal{X}$ and strings $\Delta_1, \dots, \Delta_N$ of I , a complete iteration of the SA algorithm is computed, for each $k \geq 0$, by equations

$$\mathbf{y}_\ell^k := \mathcal{F}^{i_{m(\ell)}^\ell} \circ \dots \circ \mathcal{F}^{i_2^\ell} \circ \mathcal{F}^{i_1^\ell} (\mathbf{x}^k), \quad (12)$$

$$\mathbf{y}^{k+1} := \mathcal{F}((\mathbf{y}_1^k, \dots, \mathbf{y}_N^k)). \quad (13)$$

The main advantage of this approach is to allow for computation of each vector \mathbf{y}_ℓ^k in *parallel* at each iteration k , which is possible because the step operators $\mathcal{F}^{i_1^\ell}, \dots, \mathcal{F}^{i_{m(\ell)}^\ell}$ act along each string independently.

3. Proposed algorithm

Now we are ready to define \mathcal{O}_f and \mathcal{V}_X . Let us start by defining the optimality operator $\mathcal{O}_f : \mathbb{R}_+ \times \mathbf{Y} \rightarrow \mathbf{Y}$, where \mathbf{Y} is a non-empty, closed and convex set such that $\mathbf{X} \subset \mathbf{Y} \subseteq \mathbb{R}^n$. For this, let $\mathcal{F}^{i_s^\ell} : \mathbb{R}_+ \times \mathbf{Y} \rightarrow \mathbf{Y}$ and $\mathcal{F} : \mathbf{Y}^P \rightarrow \mathbf{Y}$. Consider the set of strings $\Delta_1 = S_1, \dots, \Delta_P = S_P$ and the weight set $\{w_\ell\}_{\ell=1}^P$ as defined in the problem given in (1) with conditions (iii)-(v). Then, given $\mathbf{x} \in \mathbf{Y}$ and $\lambda \in \mathbb{R}_+$, we define

$$\mathbf{x}_{i_0^\ell} := \mathbf{x}, \quad \text{for all } \ell = 1, \dots, P, \quad (14)$$

$$\mathbf{x}_{i_s^\ell} := \mathcal{F}^{i_s^\ell}(\lambda, \mathbf{x}_{i_{s-1}^\ell}) := \mathbf{x}_{i_{s-1}^\ell} - \lambda \mathbf{g}_{i_s^\ell}, \quad s = 1, \dots, m(\ell), \quad (15)$$

$$\mathbf{x}_\ell := \mathbf{x}_{i_{m(\ell)}^\ell}, \quad \ell = 1, \dots, P, \quad (16)$$

$$\mathcal{O}_f(\lambda, \mathbf{x}) := \mathcal{F}((\mathbf{x}_1, \dots, \mathbf{x}_P)) := \sum_{\ell=1}^P w_\ell \mathbf{x}_\ell, \quad (17)$$

where $\mathbf{g}_{i_s^\ell} \in \partial f_{i_s^\ell}(\mathbf{x}_{i_{s-1}^\ell})$. Operators $\mathcal{F}^{i_s^\ell}$ in (15) correspond to the step operators in equation (12) of the SA algorithm and its definition is motivated by equation (5) of the incremental subgradient method. Function \mathcal{F} in (17) corresponds to the combination

operator in (13) and performs a weighted average of the end-points \mathbf{x}_ℓ , completing the definition of the operator \mathcal{O}_f .

Now we need to define a feasibility operator $\mathcal{V}_\mathbf{X}$. For that, we use the *subgradient projection* [4, 22, 55, 56]. Let us start noticing that every convex set $\mathbf{X} \neq \emptyset$ can be written as

$$\mathbf{X} = \bigcap_{i=1}^t \text{lev}_0(h_i), \quad (18)$$

where $\text{lev}_0(h_i) := \{\mathbf{x} \mid h_i(\mathbf{x}) \leq 0\}$. Each function $h_i : \mathbb{R}^n \rightarrow \mathbb{R}$ (t is finite) is supposed to be convex. The feasibility operator $\mathcal{V}_\mathbf{X} : \mathbb{R}^n \rightarrow \mathbb{R}^n$ is defined in [42] in the following form:

$$\mathcal{V}_\mathbf{X} := \mathcal{S}_{h_t}^{v_t} \circ \mathcal{S}_{h_{t-1}}^{v_{t-1}} \circ \dots \circ \mathcal{S}_{h_1}^{v_1}. \quad (19)$$

This definition assumes that there is $\sigma \in (0, 1]$ such that $v_i \in [\sigma, 2 - \sigma]$ for all i . Each operator $\mathcal{S}_h^v : \mathbb{R}^n \rightarrow \mathbb{R}^n$ in the previous definition is constructed using a v -relaxed version of the subgradient projection with Polyak-type step-sizes, i.e.,

$$\mathcal{S}_h^v(\mathbf{x}) := \begin{cases} \mathbf{x} - v \frac{[h(\mathbf{x})]_+ \mathbf{h}}{\|\mathbf{h}\|^2}, & \text{if } \mathbf{h} \neq \mathbf{0}; \\ \mathbf{x}, & \text{otherwise,} \end{cases} \quad (20)$$

where $v \in (0, 2)$ and $\mathbf{h} \in \partial h(\mathbf{x})$.

In order to get a better understanding of the behavior of our feasibility operator, Figure 1 shows the trajectory taken by successive applications of the operator $\mathcal{V}_\mathbf{X}$. The feasible set \mathbf{X} is the intersection of the zero sublevel sets of the following convex functions: $h_1(\mathbf{x}) = \langle \mathbf{a}, \mathbf{x} \rangle + 2\|\mathbf{x}\|_1 - 1$, $h_2(\mathbf{x}) = 3\|\mathbf{x}\|_\infty - 2.5$ and $h_3(\mathbf{x}) = \|A\mathbf{x} - \mathbf{a}\|_1 + 2\|B\mathbf{x} - \mathbf{c}\|_2 - 10$ where

$$A = \begin{bmatrix} 2 & 1 \\ -1 & 3 \end{bmatrix}, \quad B = \begin{bmatrix} 1 & 0 \\ -2 & 2 \end{bmatrix}, \quad \mathbf{a} = [2 \quad 1]^T \quad \text{and} \quad \mathbf{c} = [1 \quad -2]^T.$$

To obtain $\mathcal{V}_\mathbf{X}(\mathbf{x}) = \mathcal{S}_{h_3}^{v_3} \circ \mathcal{S}_{h_2}^{v_2} \circ \mathcal{S}_{h_1}^{v_1}(\mathbf{x})$, we compute the subgradients $\mathbf{h}_i \in \partial h_i(\mathbf{s}_{i-1})$, $i = 1, \dots, 3$, such that $\mathbf{s}_0 := \mathbf{x}$ and $\mathbf{s}_i := \mathcal{S}_{h_i}^{v_i}(\mathbf{s}_{i-1})$. We choose $[-3 \quad -2.5]^T$ as an initial point and the following relaxation parameters: $v_1 = 0.5$, $v_2 = 0.6$ and $v_3 = 0.7$.

Remark 3.1. A string-averaging version of the feasibility operator can easily be derived in the following manner. Consider Q strings $V_j := \{i_1^j, i_2^j, \dots, i_{\kappa(j)}^j\} \subset \{1, \dots, t\}$ such that $\bigcup_{j=1}^Q V_j = \{1, \dots, t\}$, where $\kappa(j)$ is the number of elements in the string V_j . Then, for each $j = 1, \dots, Q$, we define the *string feasibility operator* \mathcal{V}_j as

$$\mathcal{V}_j := \mathcal{S}_{h_{i_{\kappa(j)}^j}}^{v_{i_{\kappa(j)}^j}} \circ \mathcal{S}_{h_{i_{\kappa(j)-1}^j}}^{v_{i_{\kappa(j)-1}^j}} \circ \dots \circ \mathcal{S}_{h_{i_1^j}}^{v_{i_1^j}},$$

each satisfying for $\mathbf{y} \in \mathbf{X}_j := \bigcap_{i \in V_j} \text{lev}_0(h_i)$ and every \mathbf{x} with $d_{\mathbf{X}_j}(\mathbf{x}) \geq \delta$:

$$\|\mathcal{V}_j(\mathbf{x}) - \mathbf{y}\|^2 \leq \|\mathbf{x} - \mathbf{y}\|^2 - \epsilon_\delta^j. \quad (21)$$

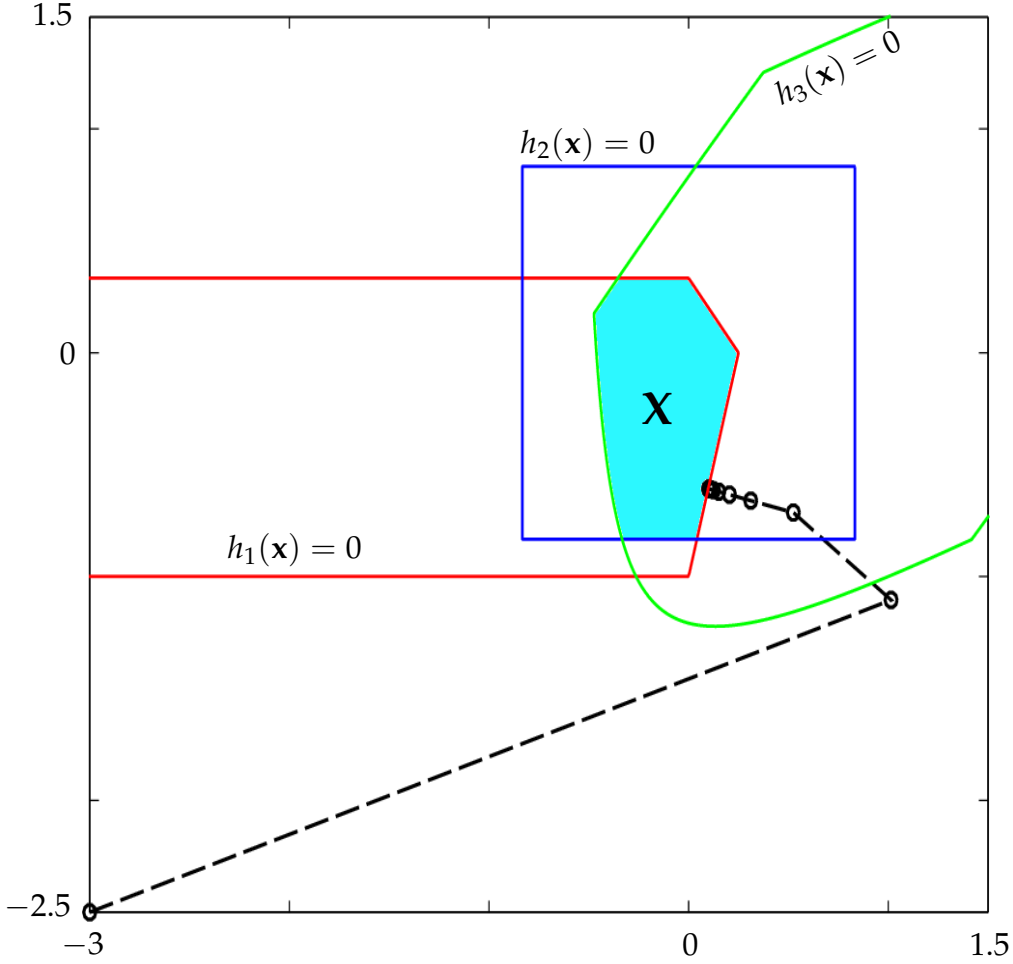


Figure 1: Ten successive applications of the feasibility operator $\mathcal{V}_{\mathbf{X}}$. The circles represent the points obtained in each application, starting from the point $[-3 \ -2.5]^T$. The dashed line describes the trajectory formed by these points.

We can then average these operators to obtain a new feasibility operator as $\tilde{\mathcal{V}}_{\mathbf{X}} := 1/Q \sum_{j=1}^Q \mathcal{V}_j$. Making use of the triangle inequality and $(\sum_{i=1}^n a_i)^2 \leq n \sum_{i=1}^n a_i^2$, we have

$$\begin{aligned} \|\tilde{\mathcal{V}}_{\mathbf{X}}(\mathbf{x}) - \mathbf{y}\|^2 &= \left\| \frac{1}{Q} \sum_{j=1}^Q [\mathcal{V}_j(\mathbf{x}) - \mathbf{y}] \right\|^2 = \frac{1}{Q^2} \left\| \sum_{j=1}^Q [\mathcal{V}_j(\mathbf{x}) - \mathbf{y}] \right\|^2 \\ &\leq \frac{1}{Q^2} \left(\sum_{j=1}^Q \|\mathcal{V}_j(\mathbf{x}) - \mathbf{y}\| \right)^2 \leq \frac{1}{Q} \sum_{j=1}^Q \|\mathcal{V}_j(\mathbf{x}) - \mathbf{y}\|^2. \end{aligned}$$

Now we notice that if \mathbf{X} is bounded, $d_{\mathbf{X}}(\mathbf{x}) \geq \delta$ implies that $\max\{d_{\mathbf{X}_j}(\mathbf{x})\} \geq \tilde{\delta} > 0$ (for weaker conditions under which the same holds, see the results in [33]). Therefore, by using (21) in the inequality above we obtain, for $\mathbf{y} \in \mathbf{X} = \bigcap_{j=1}^Q \mathbf{X}_j$ and every \mathbf{x} with

$d_{\mathbf{X}}(\mathbf{x}) \geq \delta$:

$$\|\tilde{\mathcal{V}}_{\mathbf{X}}(\mathbf{x}) - \mathbf{y}\|^2 \leq \frac{1}{Q} \sum_{j=1}^Q \left\{ \|\mathbf{x} - \mathbf{y}\|^2 - \epsilon_{\delta_j}^j \right\},$$

where $\delta_j := d_{\mathbf{X}_j}(\mathbf{x})$. Therefore:

$$\|\tilde{\mathcal{V}}_{\mathbf{X}}(\mathbf{x}) - \mathbf{y}\|^2 \leq \|\mathbf{x} - \mathbf{y}\|^2 - \tilde{\epsilon}_{\delta},$$

where $\tilde{\epsilon}_{\delta} = \min_{j \in \{1, \dots, Q\}} \{\epsilon_{\delta}^j\}$.

The above argument suggests that if the operators \mathcal{V}_j satisfy Condition 2 with \mathbf{X} replaced by \mathbf{X}_j , then its average also will satisfy Condition 2 with \mathbf{X} replaced by $\bigcap_{j=1}^Q \mathbf{X}_j$. To the best of our knowledge, the previous discussion presents a first step to generalize some of the results from [13, 15, 16] towards averaging strings of inexact projections, or more specifically, averaging of Fejér-monotone operators. We do not make use of averaged feasibility operators in this paper for clarity of presentation and also because our numerical examples can be handled in the classical way, without string averaging, since our model has few constraints. \square

With the optimality and feasibility operators already defined, we present a complete description of the algorithm we propose to solve the problem defined in (1), (i)-(v).

Algorithm 3.2 (String-averaging incremental subgradient method).

Input: Choose an initial vector $\mathbf{x}^0 \in \mathbf{Y}$ and a sequence of step-sizes $\lambda_k \geq 0$.

Iteration: Given the current iteration \mathbf{x}^k , do

Step 1. (Step operators) Compute independently for each $\ell = 1, \dots, P$:

$$\begin{aligned} \mathbf{x}_{i_0^\ell}^k &= \mathbf{x}^k, \\ \mathbf{x}_{i_s^\ell}^k &= \mathcal{F}_s^{i_s^\ell}(\lambda_k, \mathbf{x}_{i_{s-1}^\ell}^k), \quad s = 1, \dots, m(\ell), \\ \mathbf{x}_\ell^k &= \mathbf{x}_{i_{m(\ell)}^\ell}^k, \end{aligned} \tag{22}$$

where $i_s^\ell \in \Delta_\ell := S_\ell$ for each $s = 1, \dots, m(\ell)$ and $\mathcal{F}_s^{i_s^\ell}$ is defined in (15).

Step 2. (Combination operator) Use the end-points \mathbf{x}_ℓ^k obtained in Step 1 and the optimality operator \mathcal{O}_f defined in (17) to obtain:

$$\mathbf{x}^{k+1/2} = \mathcal{O}_f(\lambda_k, \mathbf{x}^k). \tag{23}$$

Step 3. Apply feasibility operator $\mathcal{V}_{\mathbf{X}}$ defined in (19) on the sub-iteration $\mathbf{x}^{k+1/2}$ to obtain:

$$\mathbf{x}^{k+1} = \mathcal{V}_{\mathbf{X}}(\mathbf{x}^{k+1/2}). \tag{24}$$

Step 4. Update k and return to Step 1.

4. Convergence analysis

Along this section, we denote $F_{S_\ell}(\mathbf{x}) = \sum_{s=1}^{m(\ell)} f_{i_s^\ell}(\mathbf{x})$ for each $\ell = 1, \dots, P$. The following subgradient boundedness assumption is key in this paper: for all ℓ and s ,

$$C_{i_s^\ell} = \sup_{k \geq 0} \left\{ \|\mathbf{g}\| \mid \mathbf{g} \in \partial f_{i_s^\ell}(\mathbf{x}^k) \cup \partial f_{i_s^\ell}(\mathbf{x}_{i_{s-1}^\ell}^k) \right\} < \infty. \quad (25)$$

Recall that Theorem 2.1 is the main tool for the convergence analysis, so we will show that each of its conditions are valid under assumption (25). We present auxiliary results in the next two lemmas.

Lemma 4.1. *Let $\{\mathbf{x}^k\}$ be the sequence generated by Algorithm 3.2 and suppose that subgradient boundedness assumption (25) holds. Then, for each ℓ and s and for all $k \geq 0$, we have*

$$(i) \quad f_{i_s^\ell}(\mathbf{x}^k) - f_{i_s^\ell}(\mathbf{x}_{i_{s-1}^\ell}^k) \leq C_{i_s^\ell} \|\mathbf{x}_{i_{s-1}^\ell}^k - \mathbf{x}^k\|. \quad (26)$$

$$(ii) \quad \|\mathbf{x}_{i_s^\ell}^k - \mathbf{x}^k\| \leq \lambda_k \sum_{r=1}^s C_{i_r^\ell}. \quad (27)$$

(iii) *For all $\mathbf{y} \in \mathbb{R}^n$, we have*

$$\left\langle \sum_{s=1}^{m(\ell)} \mathbf{g}_{i_s^\ell}^k, \mathbf{y} - \mathbf{x}^k \right\rangle \leq F_{S_\ell}(\mathbf{y}) - F_{S_\ell}(\mathbf{x}^k) + 2\lambda_k \sum_{s=2}^{m(\ell)} C_{i_s^\ell} \left(\sum_{r=1}^{s-1} C_{i_r^\ell} \right), \quad (28)$$

where $\mathbf{g}_{i_s^\ell}^k \in \partial f_{i_s^\ell}(\mathbf{x}_{i_{s-1}^\ell}^k)$.

Proof. (i) By definition of the subdifferential $\partial f_{i_s^\ell}(\mathbf{x}^k)$, we have

$$f_{i_s^\ell}(\mathbf{x}^k) - f_{i_s^\ell}(\mathbf{x}_{i_{s-1}^\ell}^k) \leq -\langle \mathbf{v}_{i_s^\ell}^k, \mathbf{x}_{i_{s-1}^\ell}^k - \mathbf{x}^k \rangle,$$

where $\mathbf{v}_{i_s^\ell}^k \in \partial f_{i_s^\ell}(\mathbf{x}^k)$. The result follows from the Cauchy-Schwarz inequality and the subgradient boundedness assumption (25).

(ii) Developing the equation $\mathbf{x}_{i_s^\ell}^k = \mathbf{x}_{i_{s-1}^\ell}^k - \lambda_k \mathbf{g}_{i_s^\ell}^k$ for each $s = 1, \dots, m(\ell)$ yields,

$$\begin{aligned} \|\mathbf{x}_{i_1^\ell}^k - \mathbf{x}^k\| &= \|\mathbf{x}^k - \lambda_k \mathbf{g}_{i_1^\ell}^k - \mathbf{x}^k\| && \leq \lambda_k C_{i_1^\ell}, \\ \|\mathbf{x}_{i_2^\ell}^k - \mathbf{x}^k\| &\leq \|\mathbf{x}_{i_1^\ell}^k - \mathbf{x}^k\| + \lambda_k \|\mathbf{g}_{i_2^\ell}^k\| && \leq \lambda_k (C_{i_1^\ell} + C_{i_2^\ell}), \\ &\vdots && \vdots \\ \|\mathbf{x}_{i_s^\ell}^k - \mathbf{x}^k\| &\leq \|\mathbf{x}_{i_{s-1}^\ell}^k - \mathbf{x}^k\| + \lambda_k \|\mathbf{g}_{i_s^\ell}^k\| && \leq \lambda_k \sum_{r=1}^s C_{i_r^\ell}. \end{aligned}$$

(iii) By Cauchy-Schwarz inequality and definition of the subdifferential $\partial f_{i_s^\ell}(\mathbf{x}_{i_{s-1}^\ell}^k)$

we have,

$$\begin{aligned}
\left\langle \sum_{s=1}^{m(\ell)} \mathbf{g}_{i_s^\ell}^k, \mathbf{y} - \mathbf{x}^k \right\rangle &= \sum_{s=1}^{m(\ell)} \langle \mathbf{g}_{i_s^\ell}^k, \mathbf{x}_{i_{s-1}^\ell}^k - \mathbf{x}^k \rangle + \sum_{s=1}^{m(\ell)} \langle \mathbf{g}_{i_s^\ell}^k, \mathbf{y} - \mathbf{x}_{i_{s-1}^\ell}^k \rangle \\
&\leq \sum_{s=1}^{m(\ell)} \|\mathbf{g}_{i_s^\ell}^k\| \|\mathbf{x}^k - \mathbf{x}_{i_{s-1}^\ell}^k\| + \sum_{s=1}^{m(\ell)} (f_{i_s^\ell}(\mathbf{y}) - f_{i_s^\ell}(\mathbf{x}_{i_{s-1}^\ell}^k)) \\
&= \sum_{s=2}^{m(\ell)} \|\mathbf{g}_{i_s^\ell}^k\| \|\mathbf{x}^k - \mathbf{x}_{i_{s-1}^\ell}^k\| + F_{S_\ell}(\mathbf{y}) - F_{S_\ell}(\mathbf{x}^k) \\
&\quad - \sum_{s=2}^{m(\ell)} (f_{i_s^\ell}(\mathbf{x}_{i_{s-1}^\ell}^k) - f_{i_s^\ell}(\mathbf{x}^k)).
\end{aligned}$$

By eqs. (26), (27) and the subgradient boundedness assumption (25) we obtain,

$$\begin{aligned}
\left\langle \sum_{s=1}^{m(\ell)} \mathbf{g}_{i_s^\ell}^k, \mathbf{y} - \mathbf{x}^k \right\rangle &\leq \sum_{s=2}^{m(\ell)} \|\mathbf{g}_{i_s^\ell}^k\| \|\mathbf{x}^k - \mathbf{x}_{i_{s-1}^\ell}^k\| + F_{S_\ell}(\mathbf{y}) - F_{S_\ell}(\mathbf{x}^k) \\
&\quad + \sum_{s=2}^{m(\ell)} \|\mathbf{v}_{i_s^\ell}^k\| \|\mathbf{x}^k - \mathbf{x}_{i_{s-1}^\ell}^k\| \\
&\leq F_{S_\ell}(\mathbf{y}) - F_{S_\ell}(\mathbf{x}^k) + \sum_{s=2}^{m(\ell)} (\|\mathbf{g}_{i_s^\ell}^k\| + \|\mathbf{v}_{i_s^\ell}^k\|) \left(\lambda_k \sum_{r=1}^{s-1} C_{i_r^\ell} \right) \\
&\leq F_{S_\ell}(\mathbf{y}) - F_{S_\ell}(\mathbf{x}^k) + 2\lambda_k \sum_{s=2}^{m(\ell)} C_{i_s^\ell} \left(\sum_{r=1}^{s-1} C_{i_r^\ell} \right).
\end{aligned}$$

□

The following Lemma is useful to analyze the convergence of the Algorithm 3.2.

Lemma 4.2. *Let $\{\mathbf{x}^k\}$ be the sequence generated by Algorithm 3.2 and suppose that assumption (25) holds. Then, there is a positive constant C such that, for all $\mathbf{y} \in \mathbf{Y} \supset \mathbf{X}$ and for all $k \geq 0$ we have*

$$\|\mathcal{O}_f(\lambda_k, \mathbf{x}^k) - \mathbf{y}\|^2 \leq \|\mathbf{x}^k - \mathbf{y}\|^2 - \frac{2}{P} \lambda_k (f(\mathbf{x}^k) - f(\mathbf{y})) + C \lambda_k^2, \quad (29)$$

Proof. Initially, we can develop equation (22) for each $\ell = 1, \dots, P$ and obtain

$\mathbf{x}_\ell^k = \mathbf{x}^k - \lambda_k \sum_{s=1}^{m(\ell)} \mathbf{g}_{i_s^\ell}^k$, where $\mathbf{g}_{i_s^\ell}^k \in \partial f_{i_s^\ell}(\mathbf{x}_{i_{s-1}^\ell}^k)$. Thus, from equation (23) we have for all $k \geq 0$,

$$\begin{aligned}
\mathcal{O}_f(\lambda_k, \mathbf{x}^k) &= \sum_{\ell=1}^P w_\ell \mathbf{x}_\ell^k \\
&= \sum_{\ell=1}^P w_\ell \left(\mathbf{x}^k - \lambda_k \sum_{s=1}^{m(\ell)} \mathbf{g}_{i_s^\ell}^k \right) \\
&= \mathbf{x}^k - \lambda_k \sum_{\ell=1}^P w_\ell \sum_{s=1}^{m(\ell)} \mathbf{g}_{i_s^\ell}^k.
\end{aligned}$$

Using the above equation we obtain for all $\mathbf{y} \in \mathbf{Y}$ and for all $k \geq 0$,

$$\begin{aligned}
\|\mathcal{O}_f(\lambda_k, \mathbf{x}^k) - \mathbf{y}\|^2 &= \left\| \mathbf{x}^k - \mathbf{y} - \lambda_k \sum_{\ell=1}^P w_\ell \sum_{s=1}^{m(\ell)} \mathbf{g}_{i_s^\ell}^k \right\|^2 \\
&= \|\mathbf{x}^k - \mathbf{y}\|^2 - 2 \left\langle \mathbf{x}^k - \mathbf{y}, \lambda_k \sum_{\ell=1}^P w_\ell \sum_{s=1}^{m(\ell)} \mathbf{g}_{i_s^\ell}^k \right\rangle + \left\| \lambda_k \sum_{\ell=1}^P w_\ell \sum_{s=1}^{m(\ell)} \mathbf{g}_{i_s^\ell}^k \right\|^2 \\
&= \|\mathbf{x}^k - \mathbf{y}\|^2 + 2\lambda_k \sum_{\ell=1}^P w_\ell \left\langle \sum_{s=1}^{m(\ell)} \mathbf{g}_{i_s^\ell}^k, \mathbf{y} - \mathbf{x}^k \right\rangle + \lambda_k^2 \left\| \sum_{\ell=1}^P w_\ell \sum_{s=1}^{m(\ell)} \mathbf{g}_{i_s^\ell}^k \right\|^2.
\end{aligned}$$

Now, using Lemma 4.1 (iii), triangle inequality and $P \sum_{\ell=1}^P w_\ell F_{S_\ell}(\mathbf{x}) = f(\mathbf{x})$ we have,

$$\begin{aligned}
\|\mathcal{O}_f(\lambda_k, \mathbf{x}^k) - \mathbf{y}\|^2 &\leq \|\mathbf{x}^k - \mathbf{y}\|^2 - 2\lambda_k \sum_{\ell=1}^P w_\ell \left[F_{S_\ell}(\mathbf{x}^k) - F_{S_\ell}(\mathbf{y}) - 2\lambda_k \sum_{s=2}^{m(\ell)} C_{i_s^\ell} \left(\sum_{r=1}^{s-1} C_{i_r^\ell} \right) \right] \\
&\quad + \lambda_k^2 \left\| \sum_{\ell=1}^P w_\ell \sum_{s=1}^{m(\ell)} \mathbf{g}_{i_s^\ell}^k \right\|^2 \\
&\leq \|\mathbf{x}^k - \mathbf{y}\|^2 - 2\lambda_k \left(\sum_{\ell=1}^P w_\ell F_{S_\ell}(\mathbf{x}^k) - \sum_{\ell=1}^P w_\ell F_{S_\ell}(\mathbf{y}) \right) \\
&\quad + 4\lambda_k^2 \sum_{\ell=1}^P w_\ell \left[\sum_{s=2}^{m(\ell)} C_{i_s^\ell} \left(\sum_{r=1}^{s-1} C_{i_r^\ell} \right) \right] + \lambda_k^2 \left(\sum_{\ell=1}^P w_\ell \sum_{s=1}^{m(\ell)} \|\mathbf{g}_{i_s^\ell}^k\| \right)^2 \\
&= \|\mathbf{x}^k - \mathbf{y}\|^2 - 2\frac{\lambda_k}{P} (f(\mathbf{x}^k) - f(\mathbf{y})) + 4\lambda_k^2 \sum_{\ell=1}^P w_\ell \left[\sum_{s=2}^{m(\ell)} C_{i_s^\ell} \left(\sum_{r=1}^{s-1} C_{i_r^\ell} \right) \right] \\
&\quad + \lambda_k^2 \left(\sum_{\ell=1}^P w_\ell \sum_{s=1}^{m(\ell)} \|\mathbf{g}_{i_s^\ell}^k\| \right)^2.
\end{aligned}$$

Finally, by subgradient boundedness assumption (25), we obtain for all $\mathbf{y} \in \mathbf{Y}$ and for all $k \geq 0$,

$$\begin{aligned}
\|\mathcal{O}_f(\lambda_k, \mathbf{x}^k) - \mathbf{y}\|^2 &\leq \|\mathbf{x}^k - \mathbf{y}\|^2 - 2\frac{\lambda_k}{P} (f(\mathbf{x}^k) - f(\mathbf{y})) \\
&\quad + \lambda_k^2 \left[4 \sum_{\ell=1}^P w_\ell \left[\sum_{s=2}^{m(\ell)} C_{i_s^\ell} \left(\sum_{r=1}^{s-1} C_{i_r^\ell} \right) \right] + \left(\sum_{\ell=1}^P w_\ell \sum_{s=1}^{m(\ell)} C_{i_s^\ell} \right)^2 \right] \\
&= \|\mathbf{x}^k - \mathbf{y}\|^2 - \frac{2}{P} \lambda_k (f(\mathbf{x}^k) - f(\mathbf{y})) + C\lambda_k^2.
\end{aligned}$$

□

The next two propositions aim at showing that, under some mild additional hypothesis, \mathcal{O}_f and \mathcal{V}_X satisfy Conditions 1-2.

Proposition 4.3. *Let $\{\mathbf{x}^k\}$ be the sequence generated by Algorithm 3.2 and suppose that subgradient boundedness assumption (25) holds. Then, if $\lambda_k \rightarrow 0^+$, the optimality operator \mathcal{O}_f satisfies Condition 1 of Theorem 2.1.*

Proof. Lemma 4.2 ensures that for all $\mathbf{x} \in \mathbf{X} \subset \mathbf{Y}$ we have,

$$\|\mathcal{O}_f(\lambda_k, \mathbf{x}^k) - \mathbf{x}\|^2 \leq \|\mathbf{x}^k - \mathbf{x}\|^2 - \frac{2}{P}\lambda_k(f(\mathbf{x}^k) - f(\mathbf{x})) + C\lambda_k^2.$$

Defining $\alpha = 2/P$ and $\rho_k = \lambda_k C \geq 0$, equation (7) is satisfied and $\rho_k \rightarrow 0$. Furthermore, by triangle inequality and subgradient boundedness assumption (25) we have,

$$\begin{aligned} \|\mathcal{O}_f(\lambda_k, \mathbf{x}^k) - \mathbf{x}^k\| &= \left\| \sum_{\ell=1}^P w_\ell \mathbf{x}_\ell^k - \mathbf{x}^k \right\| \\ &= \left\| \mathbf{x}^k - \lambda_k \sum_{\ell=1}^P w_\ell \sum_{s=1}^{m(\ell)} \mathbf{g}_{i_s^\ell}^k - \mathbf{x}^k \right\| \\ &= \lambda_k \left\| \sum_{\ell=1}^P w_\ell \sum_{s=1}^{m(\ell)} \mathbf{g}_{i_s^\ell}^k \right\| \\ &\leq \lambda_k \sum_{\ell=1}^P w_\ell \sum_{s=1}^{m(\ell)} C_{i_s^\ell}, \end{aligned}$$

implying that equation (8) is satisfied with $\gamma = \sum_{\ell=1}^P w_\ell \sum_{s=1}^{m(\ell)} C_{i_s^\ell}$. Therefore, Condition 1 is satisfied. \square

Proposition 4.4. ([42], Proposition 3.4) Let $\mathbf{x}^{k+1/2}$ given in (23) be the first element \mathbf{s}_0^k of the sequence $\{\mathbf{s}_i^k\}$, $i = 1, \dots, t$, given as $\mathbf{s}_i^k := \mathcal{S}_{h_i}^{v_i}(\mathbf{s}_{i-1}^k)$. In this sense, consider that $\mathbf{h}_i^k \in \partial h_i(\mathbf{s}_{i-1}^k)$. Suppose that for some index j , the set $\text{lev}_0(h_j)$ is bounded. In addition, consider that all sequences $\{\mathbf{h}_i^k\}$ are bounded. Then, $\mathcal{V}_\mathbf{X}$ satisfies Condition 2 of Theorem 2.1.

The main result of the paper is given next.

Corollary 4.5. Let $\{\mathbf{x}^k\}$ be the sequence generated by Algorithm 3.2 and suppose that subgradient boundedness assumption (25) holds. In addition, suppose that $\text{lev}_0(h_j)$ is bounded for some j and all sequences $\{\mathbf{h}_i^k\}$ are bounded. Then, if Conditions 3-4 of Theorem 2.1 hold, we have

$$d_{\mathbf{X}^*}(\mathbf{x}^k) \rightarrow 0 \quad \text{and} \quad \lim_{k \rightarrow \infty} f(\mathbf{x}^k) = f^*.$$

Proof. Propositions 4.3 and 4.4 state that operators \mathcal{O}_f and $\mathcal{V}_\mathbf{X}$ satisfy Conditions 1-2. Therefore, the result is obtained applying Theorem 2.1. \square

Recall that we discuss the reasonability of the Condition 4 as a hypothesis for this corollary in Remark 2.2.

5. Numerical experiments

In this section, we apply the problem formulation (1), (i)-(v) and the method given in Algorithm 3.2 to the reconstruction of tomographic images from few views, and we explore results obtained from simulated and real data to show that the method is competitive when compared with the classic incremental subgradient algorithm. Let us start with a brief description of the problem. The task of reconstructing tomographic images is related to the mathematical problem of finding a function $\psi : \mathbb{R}^2 \rightarrow \mathbb{R}$ from its line integrals along straight lines. More specifically, we desire to find ψ given the following function:

$$\mathcal{R}[\psi](\theta, t) := \int_{\mathbb{R}} \psi(t(\cos \theta, \sin \theta)^T + s(-\sin \theta, \cos \theta)^T) ds. \quad (30)$$

The application $\psi \mapsto \mathcal{R}[\psi]$ is so-called *Radon Transform* and for a fixed θ , $\mathcal{R}_\theta[\psi](t)$ is known as a *projection* of ψ . For a detailed discussion about the physical and mathematical aspects involving tomography and the definition in (30), see, for example [31, 38, 39].

We now provide an example to better understand the geometric meaning of the definition of Radon transform. We can display ψ as a picture if we assign to each value in $[0, 1]$, a grayscale such as in Figure 2-(a). Here we use an artificial image made up of a sum of indicator functions of ellipses. The bar on the right indicates the grayscale used. We also show the axes t , x , y and the integration path for a given pair (θ, t') , which appears as the dashed line segment. The t -axis directions vary according to the number of angles adopted for the reconstruction process. In general, $\theta \in [0, \pi)$ because $\mathcal{R}[\psi](\theta + \pi, -t) = \mathcal{R}[\psi](\theta, t)$. For a fixed angle θ , the projection $\mathcal{R}_\theta[\psi](t)$ is computed for each $t' \in [-1, 1]$. Figure 2-(b) shows the projections obtained for three fixed angles θ : θ_1 , θ_2 and θ_3 . Its representation given in Figure 2-(c) as an image in the $\theta \times t$ coordinate system is called *sinogram*. We also call the Radon transform at a fixed angle a *view* or *projection*.

The Radon transform models the data in a tomographic image reconstruction problem. That is, for reconstruction of the function ψ , we must go from Figure 2-(c) to the desired image in Figure 2-(a), i.e., it would be desirable to calculate the inverse \mathcal{R}^{-1} . However, as already mentioned, the Radon Transform is a compact operator and therefore its inversion is an ill-conditioned problem. In fact, for $n = 2$ and $n = 3$, Radon obtained inversion formulas involving first and second order differentiation of the data [39], respectively, implying in an unstable process due the increase of the error propagation in presence of perturbed data (when noise is present, which may occur due to width of the x-ray beam, scatter, hardening of the beam, photon statistics, detector inaccuracies, etc [31]). Other difficulties arise when using analytical solutions in practice due to, for example, the limited number of views that often occurs. This is why more sophisticated optimization models are useful, and it is desirable to use an objective function and constraints that forces the consistency of the solution to the data and guarantees stability of the solution.

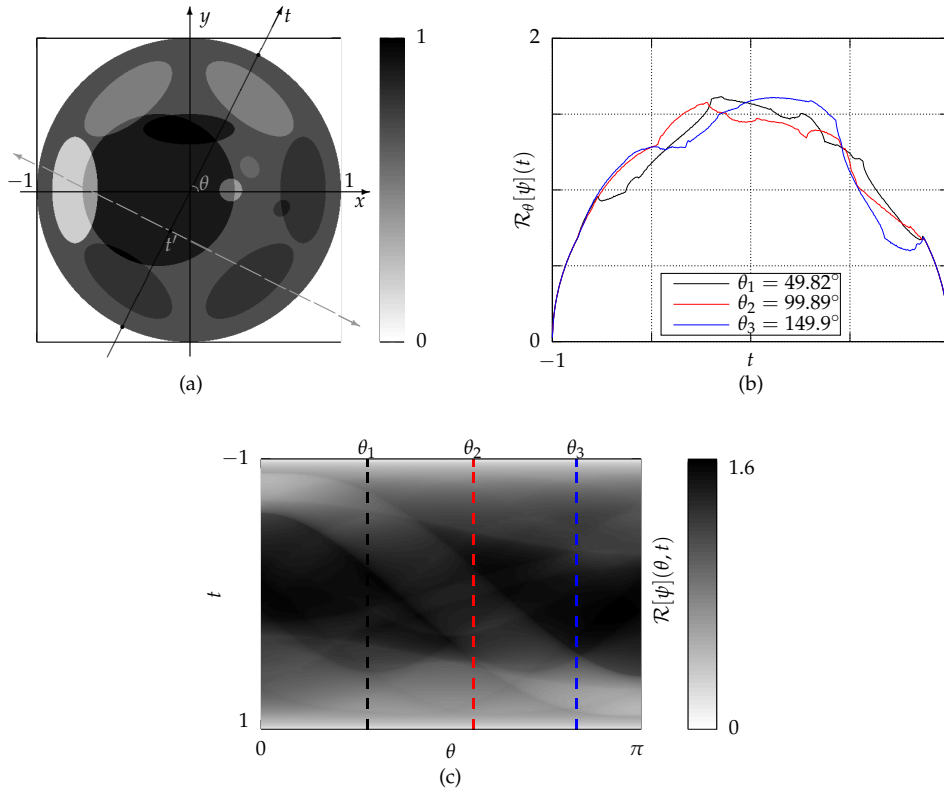


Figure 2: (a) An artificial image and the integration path for a given (θ, t') used to compute a projection $\mathcal{R}_\theta[\psi](t)$. (b) Projections for three fixed angles. (c) Sinogram obtained from image in (a).

5.1. Experimental work

In what follows we provide a detailed description of the experimental setup.

- a) *The problem:* we consider the task of reconstructing an image from few views. We use a model based in the ℓ_1 -norm of the residual associated to the linear system $R\mathbf{x} = \mathbf{b}$, where R is the $m \times n$ Radon matrix, obtained through discretization of the Radon transform in (30), $\mathbf{x} \in \mathbb{R}^n$ is the solution that we want to find, $\mathbf{b} \approx R\mathbf{x}^* \in \mathbb{R}^m$ represents the data that we have for the reconstruction (sinogram), $\mathbf{x}^* \in \mathbb{R}_+^n$ is the original image and $m \ll n$. The choice of the ℓ_1 -norm serves as a way to promote robustness to the error $\mathbf{b} - R\mathbf{x}^*$, which in the case of synchrotron illuminated tomography has relatively few very large components and many smaller ones. The small errors are related with the Poisson nature of the data, while the outliers happen because of systematic detection failure either due to dust in the ray path or to, e.g., failed detector pixels. In this manner, the following optimization problem has suitable features for the use of the Algorithm

3.2:

$$\begin{aligned}
 \min \quad & f(\mathbf{x}) = \|\mathbf{R}\mathbf{x} - \mathbf{b}\|_1 \\
 \text{s.t.} \quad & h(\mathbf{x}) = TV(\mathbf{x}) - \tau \leq 0, \\
 & \mathbf{x} \in \mathbb{R}_+^n.
 \end{aligned} \tag{31}$$

Note that the objective function $f(\mathbf{x}) = \sum_{i=1}^m |\langle \mathbf{r}_i, \mathbf{x} \rangle - b_i| = \sum_{i=1}^m f_i(\mathbf{x})$, where \mathbf{r}_i represents the i -th row of R . In comparison to (1) (i)-(v), model (31) suggests constant weights $w_\ell = 1/P$ for all $\ell = 1, \dots, P$ to satisfy conditions (iv) and (v). In our tests, we use $P = 1, \dots, 6$ and, to build the sets S_ℓ , we ordered the indices of the data randomly and then distributed in P equally sized sets (or as close to it as possible) aiming at satisfying condition (iii). We also assume that the image \mathbf{x}^* to be reconstructed has large approximately constant areas, as is often the case in tomographic images. Operator $TV : \mathbb{R}^n \rightarrow \mathbb{R}_+$ is called *total variation* and is defined by

$$TV(\mathbf{x}) = \sum_{i=1}^{r_2} \sum_{j=1}^{r_1} \sqrt{(x_{i,j} - x_{i-1,j})^2 + (x_{i,j} - x_{i,j-1})^2},$$

where $\mathbf{x} = [x_q]^T$, $q \in \{1, \dots, n\}$, $n = r_1 r_2$ and $x_{i,j} := x_{(i-1)r_1+j}$. We have also used the boundary conditions $x_{0,j} = x_{i,0} = 0$ and $\tau = TV(\mathbf{x}^*)$.

- b) *Data generation*: for this simulated experiment, we have considered the reconstruction of the Shepp-Logan phantom [36]. In Figure 3, we show this image using a grayscale version with resolution of 256×256 . This resolution will also be used for the reconstruction. For the vector \mathbf{b} that contains the data

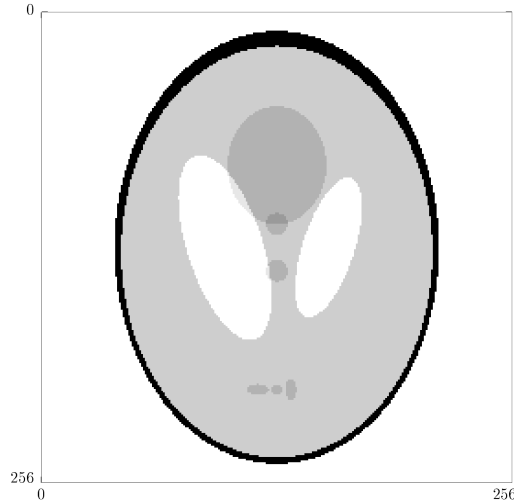


Figure 3: Shepp-Logan phantom with resolution 256×256 .

to be used in the reconstruction, we need an efficient routine for calculating the product $R\mathbf{x}$. We consider 24 equally spaced angular projections with each

sampled at 256 equally spaced points. We also consider reconstruction of images affected by Poisson noise, i.e., we execute the algorithms using data that was generated as samples of a Poisson random variable having as parameter the exact Radon Transform of the scaled phantom:

$$\mathbf{b} \sim \text{Poisson}(\kappa \mathcal{R}[\psi](\theta, t)), \quad (32)$$

where the scale factor $\kappa > 0$ is used to control the simulated photon count, i.e., the noise level. Figure 4 shows the result obtained for $\mathbf{b} = R\mathbf{x}^*$, where \mathbf{x}^* is the Shepp-Logan phantom, in both cases, i.e., with and without noise in the data.

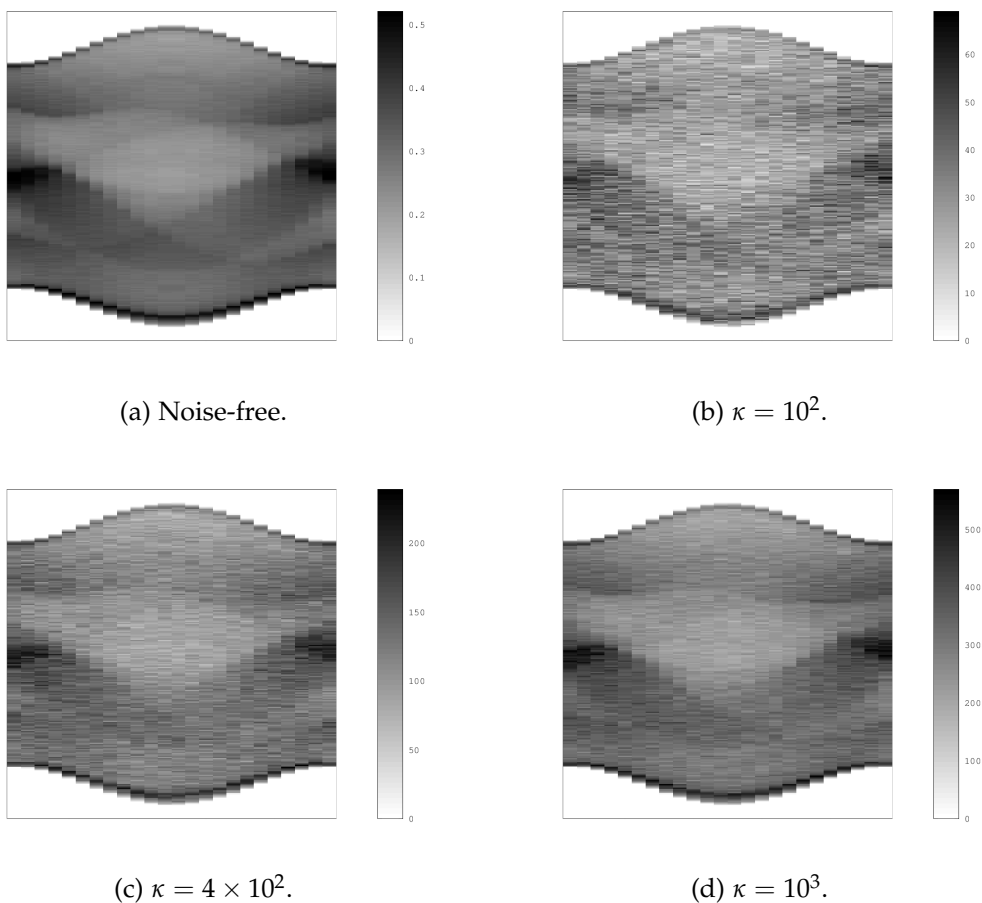


Figure 4: Sinograms obtained from Radon transform of Shepp-Logan phantom. Only 24 equally spaced angular projections are taken, each sampled at 256 equally spaced points.

c) *Initial image*: for the initial image \mathbf{x}^0 , we seek an uniform vector that somehow has information from data obtained by the Radon Transform of Shepp-Logan head phantom. For that, we use an initial image that satisfy $\sum_{i=1}^m \langle \mathbf{r}_i, \mathbf{x}^0 \rangle = \sum_{i=1}^m b_i$. Therefore, supposing $x_j^0 = \zeta$ for all $j = 1, \dots, n$, we can compute ζ by

$$\zeta = \frac{\sum_{i=1}^m b_i}{\sum_{i=1}^m \langle \mathbf{r}_i, \mathbf{1} \rangle}, \quad (33)$$

where $\mathbf{1}$ is the n -vector whose components are all equal to 1.

d) *Applying Algorithm 3.2*: step-size sequence $\{\lambda_k\}$ was determined by the formula

$$\lambda_k = (1 - \rho c_k) \frac{\lambda_0}{\alpha k^s / P + 1}, \quad (34)$$

where the sequence c_k starts with $c_0 = 0$ and the following terms are given by

$$c_k = \frac{\langle \mathbf{x}^{k-1/2} - \mathbf{x}^{k-1}, \mathbf{x}^k - \mathbf{x}^{k-1/2} \rangle}{\|\mathbf{x}^{k-1/2} - \mathbf{x}^{k-1}\| \|\mathbf{x}^k - \mathbf{x}^{k-1/2}\|}.$$

Each c_k is the cosine of the angle between the directions taken by optimality and feasibility operators in the previous iteration. Thus, the factor $(1 - \rho c_k)$ serves as an empirical way to prevent oscillations. Finally, we use $\lambda_0 = \mu \|\mathbf{R}\mathbf{x}^0 - \mathbf{b}\|_1 / \|\mathbf{g}^0\|^2$, where μ is the number of parcels in which the sum is divided and \mathbf{g}^0 is a subgradient of objective function in \mathbf{x}^0 . Other free parameters in (34) were tuned and set to: $\rho = 0.999$, $s = 0.51$ and $\alpha = 1.0$.

Now we need to calculate the subgradients for the objective function and TV. Since the vector

$$\mathbf{sign}(\mathbf{x}) = [u_i]^T, \quad \text{such that } u_i := \begin{cases} 1, & \text{if } x_i > 0, \\ 0, & \text{if } x_i = 0, \\ -1, & \text{otherwise} \end{cases}$$

belongs to the set $\partial \|\mathbf{x}\|_1$, then the theorem 4.2.1, p. 263 in [32] guarantees that

$$\mathbf{R}^T \mathbf{sign}(\mathbf{R}\mathbf{x} - \mathbf{b}) \in \partial \|\mathbf{R}\mathbf{x} - \mathbf{b}\|_1,$$

and this subgradient will be used in our experiments. In particular, for each $k \geq 0$, $\ell = 1, \dots, P$ and $s = 1, \dots, m(\ell)$ we use

$$\mathbf{g}_{i_s^\ell}^k = \begin{cases} \mathbf{r}_{i_s^\ell}, & \text{if } \langle \mathbf{r}_{i_s^\ell}, \mathbf{x}_{i_{s-1}^\ell}^k \rangle - b_{i_s^\ell} > 0, \\ -\mathbf{r}_{i_s^\ell}, & \text{if } \langle \mathbf{r}_{i_s^\ell}, \mathbf{x}_{i_{s-1}^\ell}^k \rangle - b_{i_s^\ell} < 0, \\ 0, & \text{otherwise.} \end{cases} \quad (35)$$

A subgradient $\mathbf{h} = [t_{i,j}]$ for $h(\mathbf{x}) = TV(\mathbf{x}) - \tau$ can be computed by

$$t_{i,j} = \frac{2x_{i,j} - x_{i,j-1} - x_{i-1,j}}{\sqrt{(x_{i,j} - x_{i,j-1})^2 + (x_{i,j} - x_{i-1,j})^2}} + \frac{x_{i,j} - x_{i,j+1}}{\sqrt{(x_{i,j+1} - x_{i,j})^2 + (x_{i,j+1} - x_{i-1,j+1})^2}} + \frac{x_{i,j} - x_{i+1,j}}{\sqrt{(x_{i+1,j} - x_{i,j})^2 + (x_{i+1,j} - x_{i+1,j-1})^2}}, \quad (36)$$

where, if any denominator is zero, we annul the correspondent parcel.

Once we have determined the strings by setting $\Delta_1 = S_1, \dots, \Delta_P = S_P$ and weights ($w_\ell = 1/P$ for all ℓ), the step-size sequence λ_k in (34), initial image \mathbf{x}^0 in (33) and subgradients $\mathbf{g}_{i_s^\ell}^k \in \partial f_{i_s^\ell}(\mathbf{x}_{i_{s-1}^\ell}^k)$ in (35), optimality operator \mathcal{O}_f (14)-(17) can be

applied. By considering the subdifferential of $\|\mathbf{x}\|_1$, it is clear that $\partial f(\mathbf{x})$ is uniformly bounded, ensuring that assumption (25) holds. Moreover, since $\rho \in [0, 1)$, $\alpha > 0$, $s \in (0, 1]$ and $c_k \in [-1, 1]$, by Cauchy-Schwarz inequality we can ensure that $\lambda_k > 0$ and that Condition 3 of Theorem 2.1 holds.

Using $\mathbf{h} \in \partial h(\mathbf{x})$ defined in (36), operator \mathcal{S}_h^ν can be computed by equation (20), such that, in our tests, we use $\nu = 1$. The feasibility operator is thus given by $\mathcal{V}_\mathbf{x} = \mathcal{P}_{\mathbb{R}_+^n} \circ \mathcal{S}_h^\nu$ (see equation (19)). The projection step can be regarded as a special case of the operator \mathcal{S}_g^ν with $\nu = 1$ and $g = d_{\mathbb{R}_+^n}$. It is easy to see that $\mathcal{V}_\mathbf{x}$ defined in this way satisfies the conditions established in the Proposition 4.4.

In conclusion, once $\|R\mathbf{x} - \mathbf{b}\|_1 \geq 0$, Corollary 2.7 in [42] implies that $\{d_\mathbf{x}(\mathbf{x}^k)\} \rightarrow 0$ (the sequence is bounded). Since $\partial f(\mathbf{x})$ is uniformly bounded, we have that $[f(\mathcal{P}_\mathbf{x}(\mathbf{x}^k)) - f(\mathbf{x}^k)]_+ \rightarrow 0$ and Condition 4 of Theorem 2.1 holds. Thus, Corollary 4.5 can be applied ensuring convergence of the Algorithm 3.2.

5.2. Image reconstruction analysis

To run the experiments, we used a computer with processor Intel Core i7-4790 CPU @ 3.60 GHz x8 and 16 GB of memory. The operating system used was Linux and the implementation was realized in C++. Figure 5 shows the decrease of the objective function with respect to computation time to compare convergence speed and image quality in the performed reconstructions. Furthermore, in order to obtain a more meaningful analysis, we consider the graphic of the total variation $TV(\mathbf{x})$ and the *relative squared error*,

$$RSE(\mathbf{x}) = \frac{\|\mathbf{x} - \mathbf{x}^*\|^2}{\|\mathbf{x}^*\|^2}.$$

Note that the *RSE* metric requires information on the desired image. Also we show graphs of $TV(\mathbf{x}^k)$ as function of $f(\mathbf{x}^k)$.

When we use $P = 2, \dots, 6$ (algorithm is executed with 2-6 strings), it is possible to observe a faster decrease in the values of the objective function $f(\mathbf{x}^k)$ as the running time increases, if compared to the case where $P = 1$. Since there is no guarantee that algorithm produces a descent direction in each iteration, it is important to note that, in some of the tests, the intensity of the oscillation, i.e., $f(\mathbf{x}^{k+1}) - f(\mathbf{x}^k)$ for $f(\mathbf{x}^{k+1}) > f(\mathbf{x}^k)$, decreases as the number of strings increases (note, for example, the algorithm performance with 5 and 6 strings, from 0 to about 40 seconds). A similar behavior can be noted for values $TV(\mathbf{x}^k)$. For 4-6 strings, the algorithm is able to provide images with a more appropriate *TV* level, approaching the feasible region more quickly. Even if closer to satisfying the constraints, for methods with a larger number of strings, the values of $RSE(\mathbf{x}^k)$ and of the objective function decrease with lower intensity oscillations and reach lower values within the same computation time. Interestingly, the experiments with noisy data show that the algorithm generates a sharp decrease in the intensity of oscillation precisely where image quality seems to reach a good level. The study of conditions under which we can establish a stopping

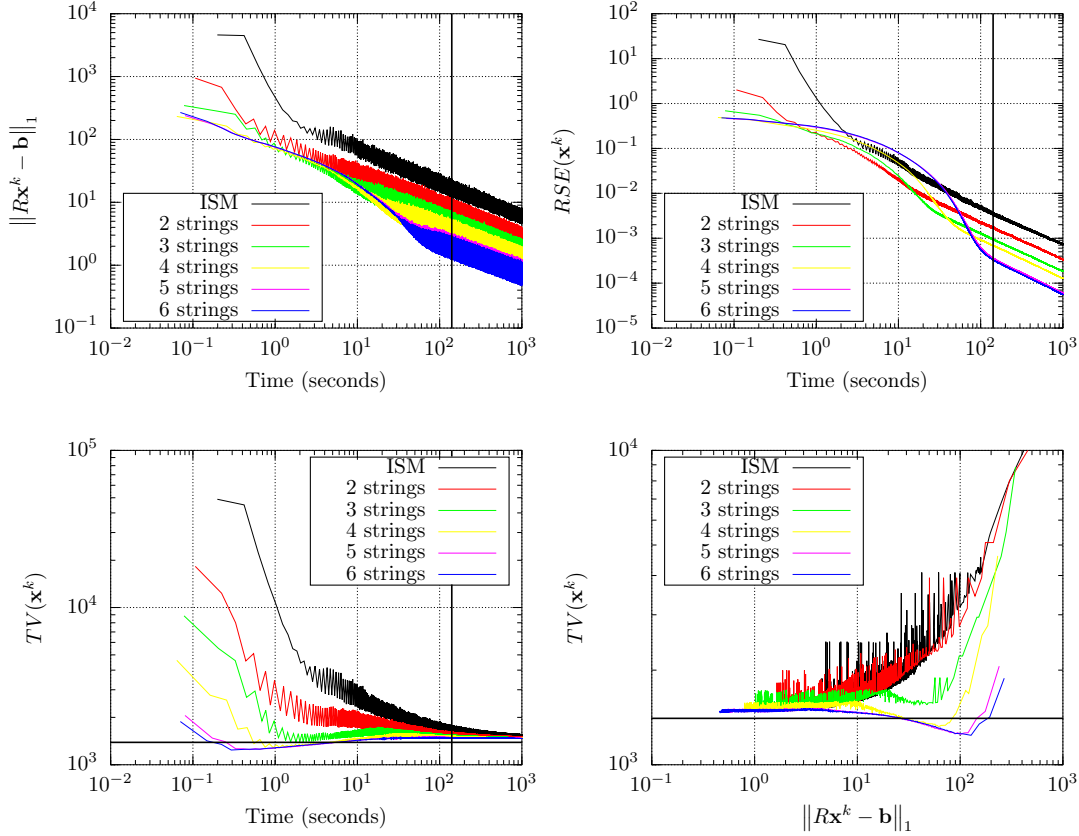


Figure 5: Decrease of the objective function, TV and RSE in a noise-free condition. Comparing ISM (1 string) with algorithms that use 2-6 strings, executed in parallel, lower values are reached for the objective and RSE functions. For TV , we get an oscillation with lower intensity (especially when we used 4-6 strings). Note that solid horizontal lines on TV graph represent the target value $\tau = TV(\mathbf{x}^*)$. The solid vertical lines show, for a fixed computation time, that both functions values are decreasing with respect to the number of strings P . Figure 6 shows the reconstructed images by the algorithms for this fixed computation time. In the bottom right figure, note that TV values appear to represent, at many fixed levels of residual ℓ_1 -norm, a decreasing function of the number of strings.

criterion for the algorithm are left for future research, perhaps taking advantage of this kind of phenomenon.

The quality of the reconstruction is significantly affected by the increase in the number of strings. Figure 6 shows the reconstructed images obtained in the experiments. There is a clear difference in the quality of reconstruction for ISM and algorithms with 2-6 strings. For 5 and 6 strings the reconstruction is visually perfect.

Figures 7, 8 and 9 show plots similar to those in Figure 5 but now under different relative noise levels, which was computed as $\|\mathbf{b} - \mathbf{b}^\dagger\| / \|\mathbf{b}^\dagger\|$, where \mathbf{b}^\dagger is the vector

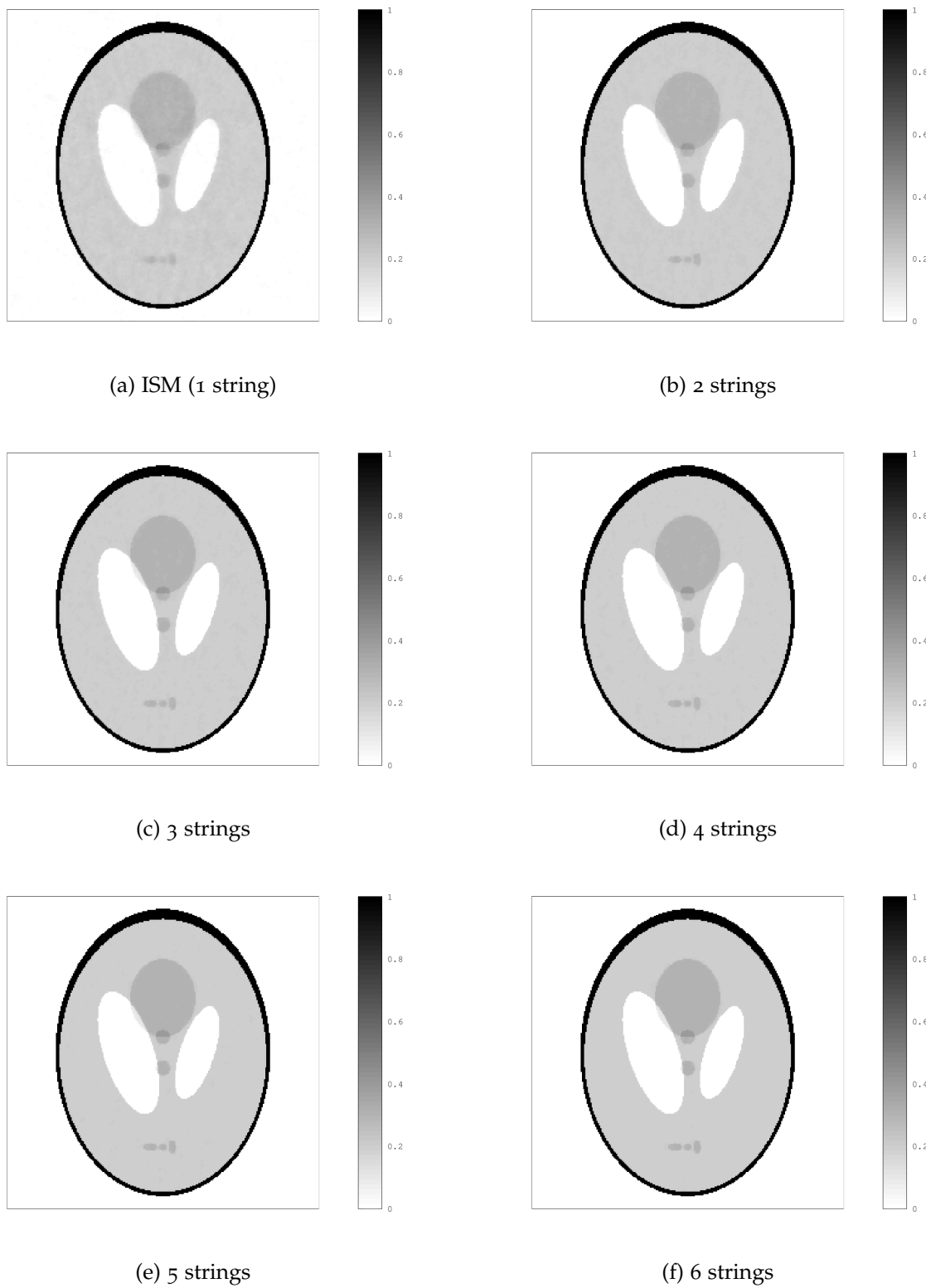


Figure 6: Reconstructed images obtained in the computation time mentioned in the Figure 5.

that contains the ideal data. We can note that the behavior of algorithm is similar

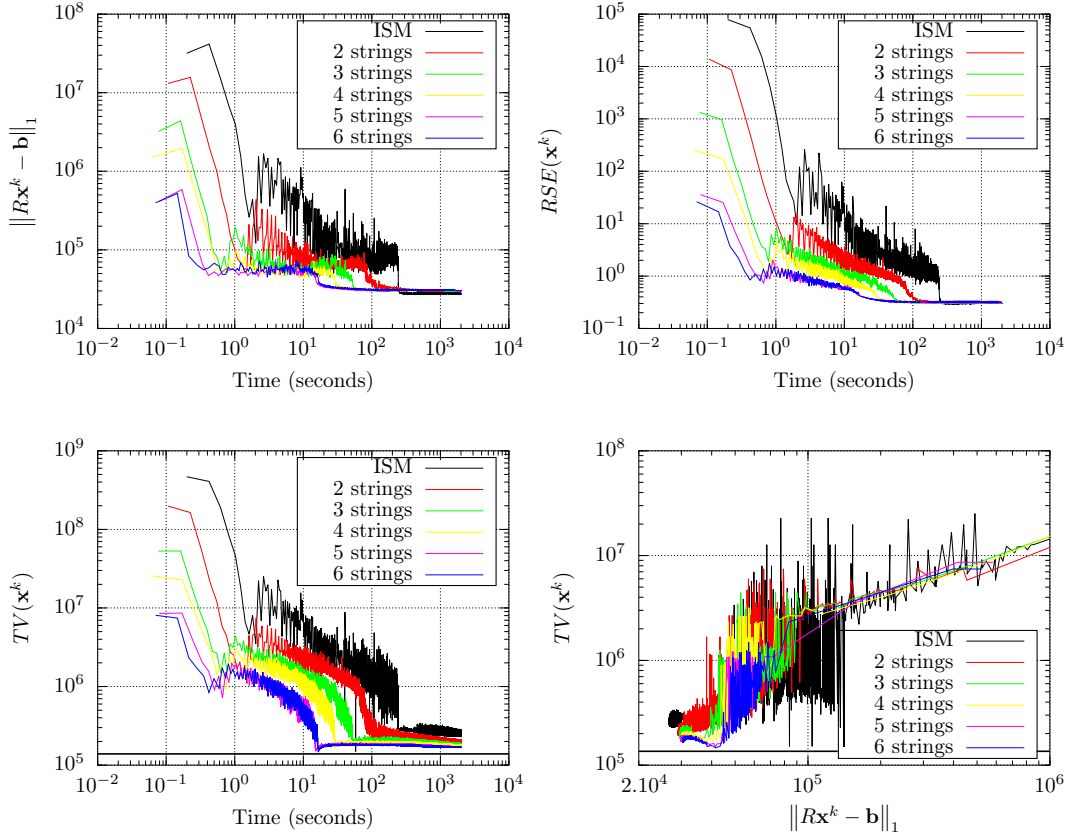


Figure 7: Test with 17.8% of relative noise.

to the previous case. Algorithms with larger number of strings reach results that the ISM takes longer to reach. Furthermore, oscillations with lower intensity can be noted, especially for 5 and 6 strings. Figure 10 shows the reconstructed images obtained by ISM and method with 6 strings according to the following rule: we set an objective function value and seek the first iteration to fall below this threshold for each method. Table 1 provides the running time and total variation for each case. These data confirm a good performance of the algorithm with string averaging, in the sense that, for fixed values of objective function, algorithm running with 6 strings provides images in which quality appears to be improved (or at least is similar) with lower running time, if compared against ISM.

5.3. Tests with real data

Tomographic data was obtained by synchrotron radiation illumination of eggs of fishes of the species *Prochilodus lineatus* collected at the Madeira river's bed at Brazilian National Synchrotron Light Laboratory's (LNLS) facility. The eggs had

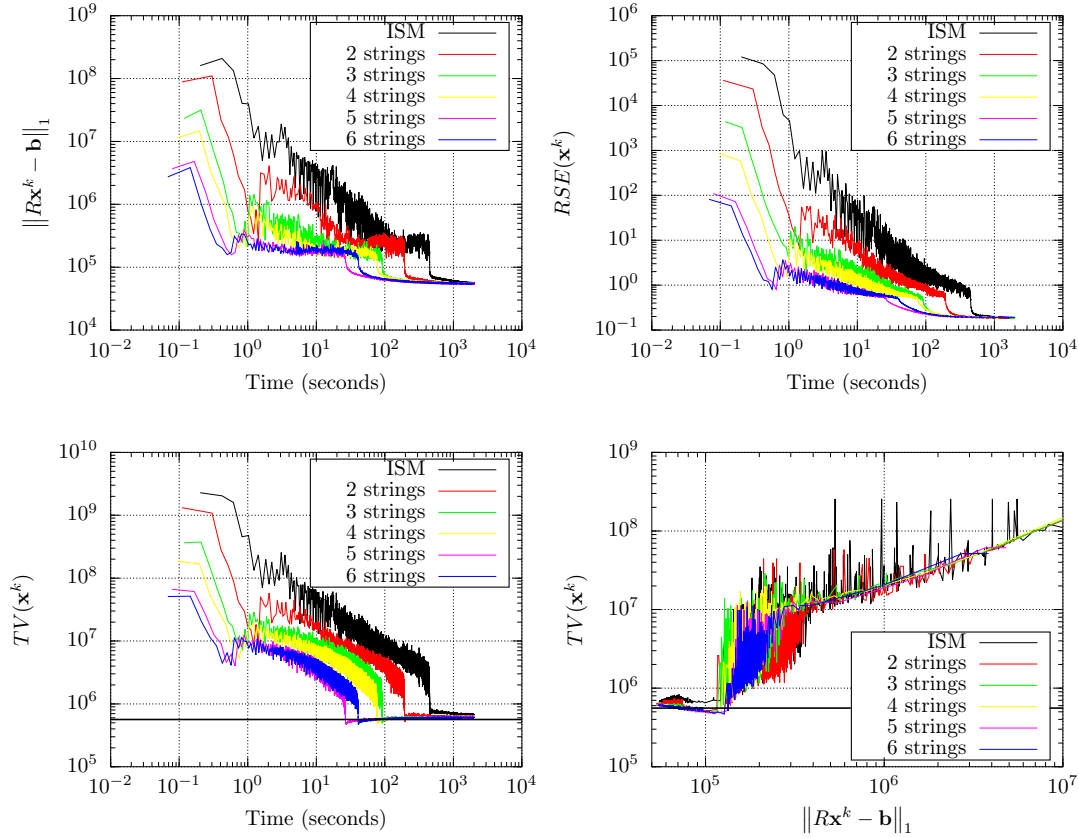


Figure 8: Test with 8.78% of relative noise.

Method / Noise / $f(\mathbf{x})$	Time (s)	$TV(\mathbf{x})$
ISM / 17.8% / 3.194×10^4	2.45×10^2	2.7×10^5
$P = 6$ / 17.8% / 3.191×10^4	6.0×10^1	1.82×10^5
ISM / 8.78% / 6.070×10^4	7.11×10^2	6.91×10^5
$P = 6$ / 8.78% / 6.093×10^4	1.5×10^2	5.87×10^5
ISM / 5.65% / 9.889×10^4	1.87×10^3	1.48×10^6
$P = 6$ / 5.65% / 9.889×10^4	2.2×10^2	1.36×10^6

Table 1: Running time and total variation obtained by ISM and method with 6 strings under conditions of Poisson relative noise used in the tests for some fixed values of objective function.

been previously embedded in formaldehyde in order to prevent decay, but were later fixed in water within a borosilicate capillary tube for the scan. The sample was placed between the x-ray source and a photomultiplier coupled to a CCD capable of recording the images. After each radiographic measurement, the sample was rotated

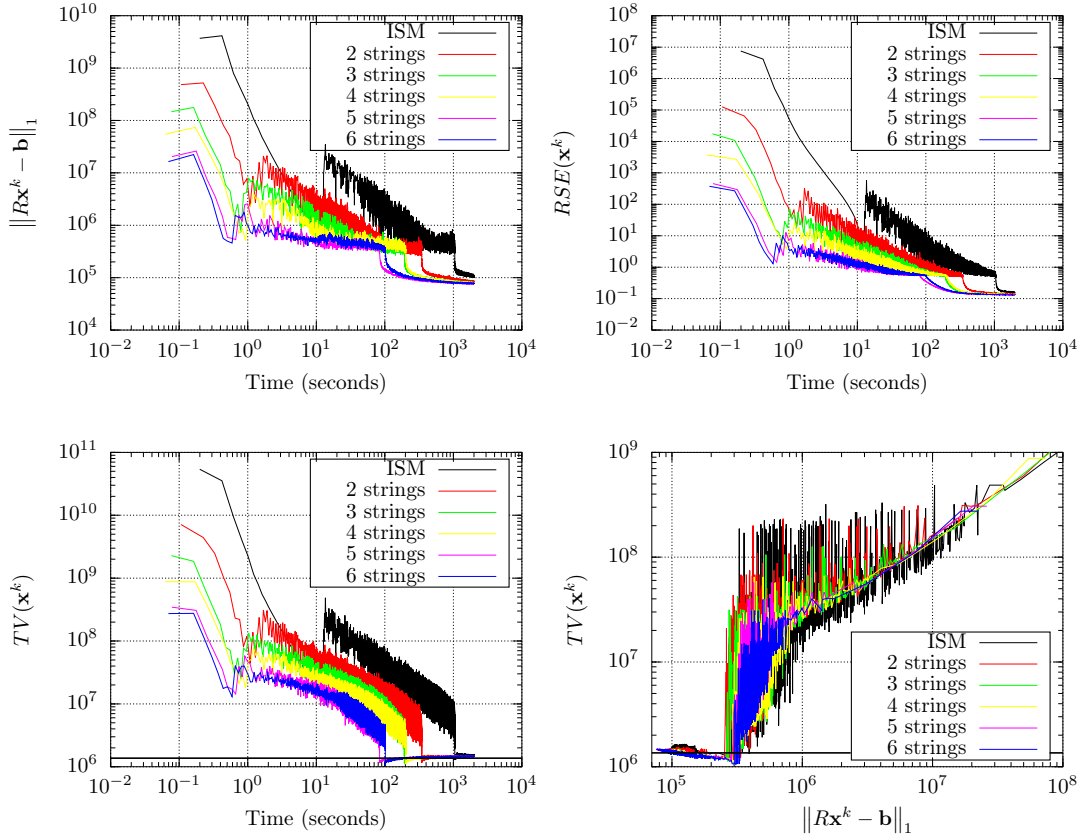


Figure 9: Test with 5.65% of relative noise.

by a fixed amount and a new measurement was made.

A monochromator was added to the experiment to filter out low energy photons and avoid overheating of the soft eggs and the embedding water. This leads to a low photon flux, which increased the required exposure time to 20 seconds for each projection measurement. Each of this radiographic image was 2048×2048 pixels covering an area of $0.76 \times 0.76 \text{mm}^2$. Given the high measurement duration of each projection, for the experiment to have a reasonable time span, we have collected only 200 views in the 180° range, leading to slice tomographic datasets (sinograms) each of dimension 2048×200 (see Figure 11).

In this experiment, we use $\tau = 5 \times 10^4$, $\nu = 1.5$ and the other parameters ρ , α and s were the same as in the previous experiment. Furthermore, to avoid high step-size values, we multiply the initial step-size λ_0 by 0.25. Figure 12 shows the plot of TV as function of residual ℓ_1 -norm. Better quality reconstructions are generated by the algorithm that uses 6 strings. Figure 13 shows the images obtained by reconstruction. By considering that the eggs were immersed in water, which has homogeneous attenuation value, we can conclude that image in Figure 13-(b) has less artifacts. Figure 14 shows profile lines of the reconstructed images in Figure 13. Note that

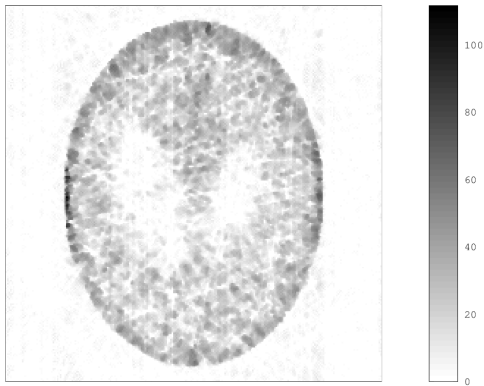
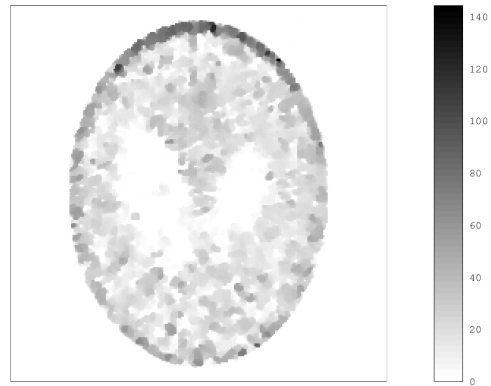
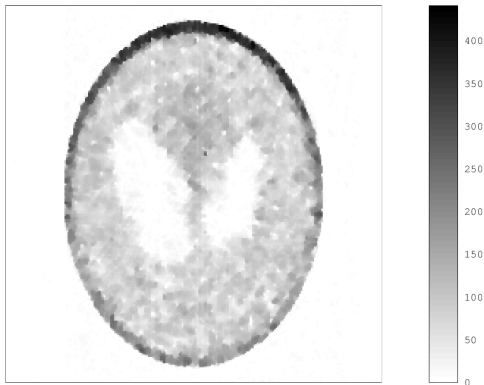
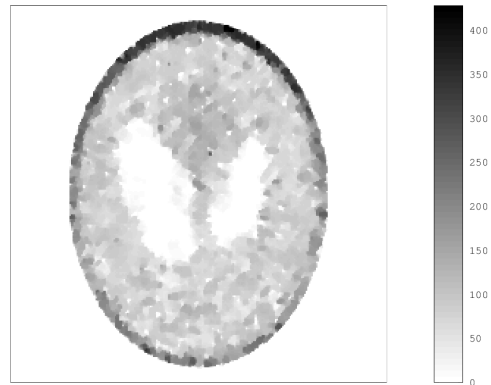
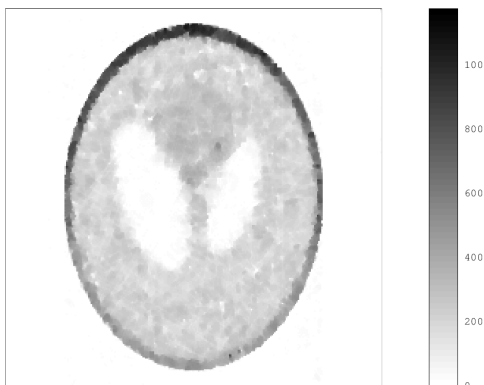
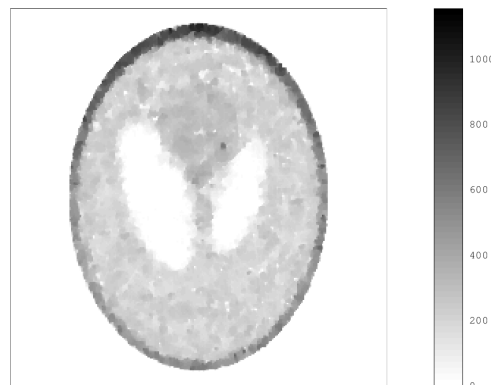
(a) ISM / 17.8% / 3.194×10^4 .(b) $P = 6$ / 17.8% / 3.191×10^4 .(c) ISM / 8.78% / 6.070×10^4 (d) $P = 6$ / 8.78% / 6.093×10^4 .(e) ISM / 5.65% / 9.889×10^4 .(f) $P = 6$ / 5.65% / 9.889×10^4 .

Figure 10: Reconstructed images obtained in the tests with Poisson noise. Items (a)-(f) exhibit: method / relative noise / $f(x)$. Table 1 shows running time and total variation obtained in each case.

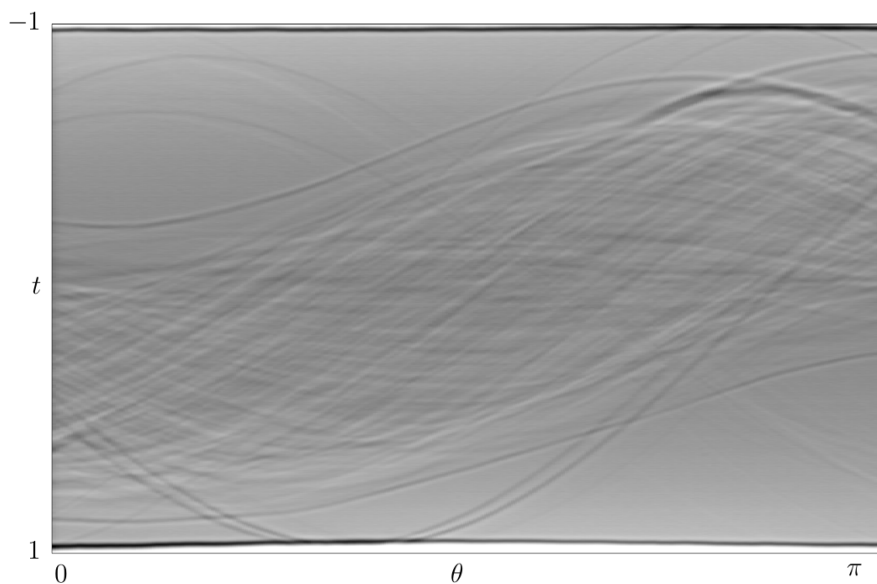


Figure 11: Sinogram obtained by synchrotron radiation illumination of eggs of fishes.

algorithm running with 6 strings presents a reconstruction with less overshoot and more smoothness than ISM.

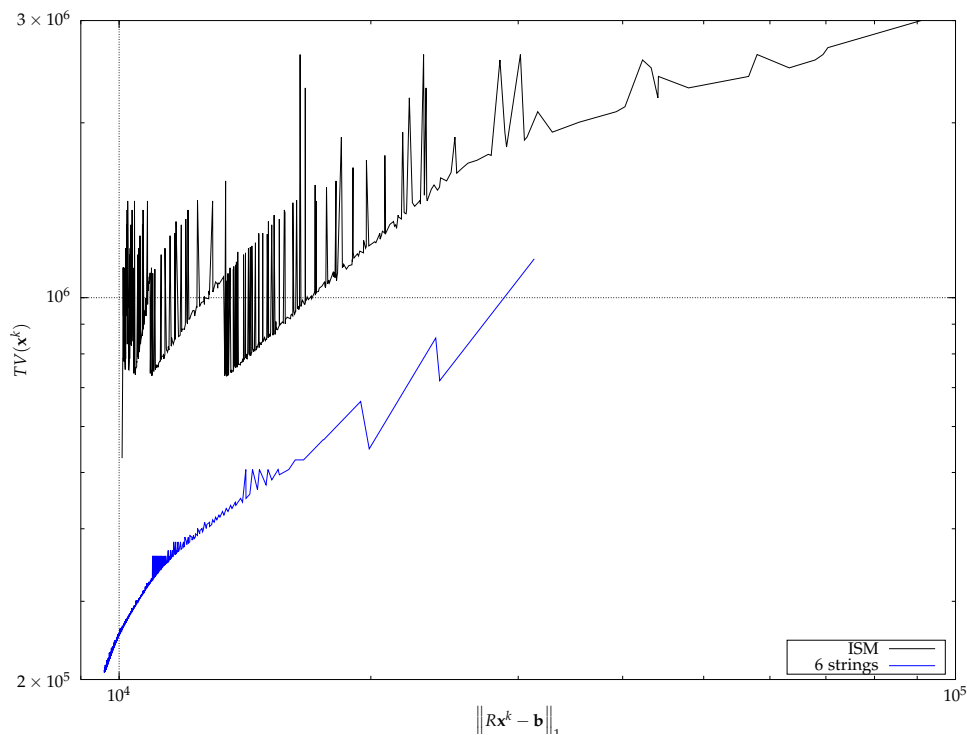


Figure 12: Total variation as function of the residual ℓ_1 -norm for the experiment using eggs of fishes. Note that the method with 6 strings provides lower values for total variation with a lower oscillation level.

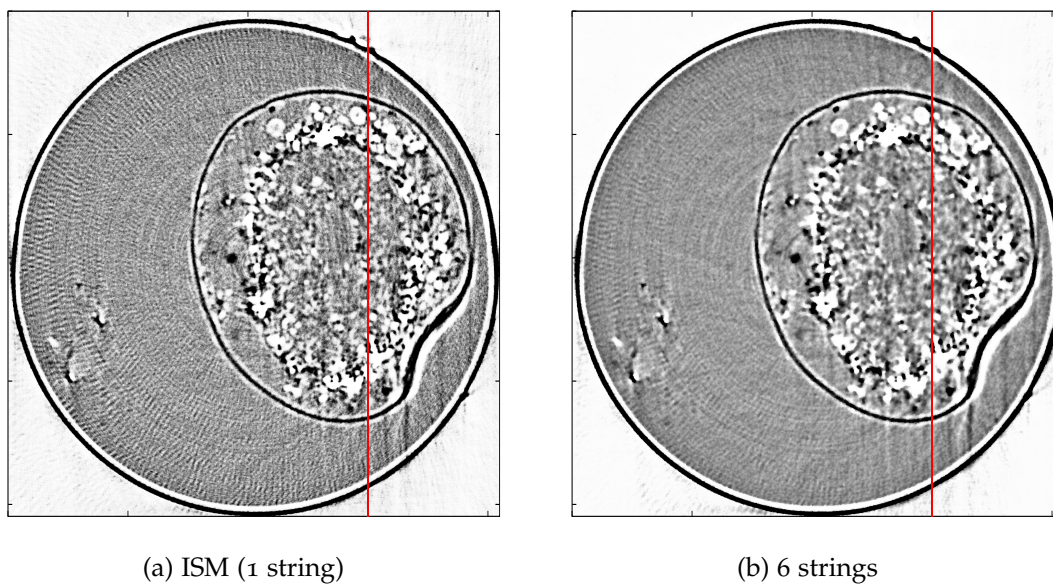


Figure 13: Reconstructed images from sinogram given in Figure 11. The vertical solid red lines show where the profiles of Figure 14 were taken from.

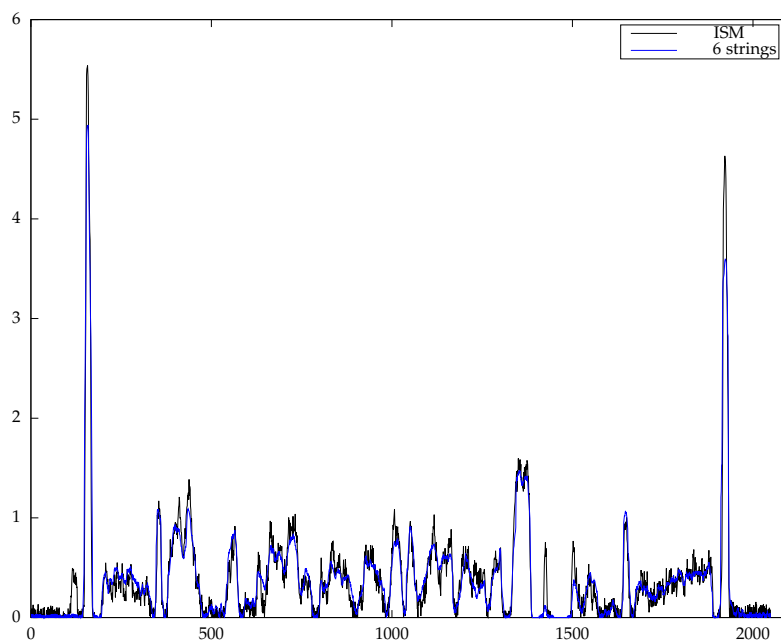


Figure 14: Profile lines from images in Figure 13.

6. Final comments

We have presented a new String-Averaging Incremental Subgradients family of algorithms. The theoretical convergence analysis of the method was established and experiments were performed in order to assess the effectiveness of the algorithm. The method featured a good performance in practice, being able to reconstruct images with superior quality when compared to classical incremental subgradient algorithms. Furthermore, algorithmic parameters selection was shown to be robust across a range of tomographic experiments. The discussed theory involves solving non-smooth constrained convex optimization problems and, in this sense, more general models can be numerically addressed by the presented method. Future work may be related to the application of the string-averaging technique in incremental subgradient algorithms with stochastic errors, such as those that appear in [50] and [51].

Acknowledgements

We would like to thank the LNLS for providing the beam time for the tomographic acquisition, obtained under proposal number 17338. We also want to thank Prof. Marcelo dos Anjos (Federal University of Amazonas) for kindly providing the fish egg samples used in the presented experimentation. RMO was partially funded by FAPESP Grant 2015/10171-2. ESH was partially funded by FAPESP Grants 2013/16508-3 and 2013/07375-0 and CNPq Grant 311476/2014-7. EFC was funded by FAPESP under Grant 13/19380-8 and CNPq under Grant 311290/2013-2.

References

- [1] AHN, S., AND FESSLER, J. A. Globally convergent image reconstruction for emission tomography using relaxed ordered subsets algorithms. *Medical Imaging, IEEE Transactions on* 22, 5 (2003), 613–626.
- [2] ANTHOINE, S., AUJOL, J.-F., BOURSIER, Y., AND MELOT, C. Some proximal methods for Poisson intensity CBCT and PET. *Inverse Problems and Imaging* 6, 4 (2012), 565–598.
- [3] BAUSCHKE, H. H., AND BORWEIN, J. M. On projection algorithms for solving convex feasibility problems. *SIAM Review* 38, 3 (1996), 367–426.
- [4] BAUSCHKE, H. H., COMBETTES, P. L., AND KRUK, S. G. Extrapolation algorithm for affine-convex feasibility problems. *Numerical Algorithms* 41, 3 (2006), 239–274.
- [5] BECK, A., AND TEOULLE, M. Fast gradient-based algorithms for constrained total variation image denoising and deblurring problems. *IEEE Transactions on Image Processing* 18, 11 (2009), 2419–2434.
- [6] BECK, A., AND TEOULLE, M. A fast iterative shrinkage-thresholding algorithm for linear inverse problems. *SIAM Journal on Imaging Sciences* 2, 1 (2009), 183–202.

- [7] BERTSEKAS, D. P. A new class of incremental gradient methods for least squares problems. *SIAM Journal on Optimization* 7, 4 (1997), 913–926.
- [8] BERTSEKAS, D. P. *Nonlinear programming*. Athena scientific, Belmont, MA, 1999.
- [9] BERTSEKAS, D. P., AND TSITSIKLIS, J. N. Gradient convergence in gradient methods with errors. *SIAM Journal on Optimization* 10, 3 (2000), 627–642.
- [10] BLATT, D., HERO, A. O., AND GAUCHMAN, H. A convergent incremental gradient method with a constant step size. *SIAM Journal on Optimization* 18, 1 (2007), 29–51.
- [11] BREDIES, K. A forward-backward splitting algorithm for the minimization of non-smooth convex functionals in Banach space. *Inverse Problems* 25, 1 (2009), 015005.
- [12] BROWNE, J., AND DE PIERRO, A. R. A row-action alternative to the EM algorithm for maximizing likelihoods in emission tomography. *Medical Imaging, IEEE Transactions on* 15, 5 (1996), 687–699.
- [13] CENSOR, Y., ELFVING, T., AND HERMAN, G. T. Averaging strings of sequential iterations for convex feasibility problems. *Inherently parallel algorithms in feasibility and optimization and their applications* 8 (2001), 101–113.
- [14] CENSOR, Y., AND TOM, E. Convergence of string-averaging projection schemes for inconsistent convex feasibility problems. *Optimization Methods & Software* 18 (2003), 543–554.
- [15] CENSOR, Y., AND ZASLAVSKI, A. J. Convergence and perturbation resilience of dynamic string-averaging projection methods. *Computational Optimization and Applications* 54, 1 (2013), 65–76.
- [16] CENSOR, Y., AND ZASLAVSKI, A. J. String-averaging projected subgradient methods for constrained minimization. *Optimization Methods and Software* 29, 3 (2014), 658–670.
- [17] CHEN, G. H.-G., AND ROCKAFELLAR, R. T. Convergence rates in forward-backward splitting. *SIAM Journal on Optimization* 7, 2 (1997), 421–444.
- [18] CHOUZENOUX, E., JEZIERSKA, A., PESQUET, J.-C., AND TALBOT, H. A majorize-minimize subspace approach for $\ell_2 - \ell_0$ image regularization. *SIAM Journal on Imaging Sciences* 6, 1 (2013), 563–591.
- [19] CHOUZENOUX, E., PESQUET, J. C., TALBOT, H., AND JEZIERSKA, A. A memory gradient algorithm for $\ell_2 - \ell_0$ regularization with applications to image restoration. In *2011 18th IEEE International Conference on Image Processing* (2011), pp. 2717–2720.
- [20] CHOUZENOUX, E., ZOLYNIK, F., GOUILLART, E., AND TALBOT, H. A majorize-minimize memory gradient algorithm applied to X-ray tomography. In *2013 IEEE International Conference on Image Processing* (2013), pp. 1011–1015.

- [21] COMBETTES, P. L. Inconsistent signal feasibility problems: Least-squares solutions in a product space. *Signal Processing, IEEE Transactions on* 42, 11 (1994), 2955–2966.
- [22] COMBETTES, P. L. Convex set theoretic image recovery by extrapolated iterations of parallel subgradient projections. *Image Processing, IEEE Transactions on* 6, 4 (1997), 493–506.
- [23] COMBETTES, P. L., AND PESQUET, J.-C. A proximal decomposition method for solving convex variational inverse problems. *Inverse Problems* 24, 6 (2008), 065014.
- [24] COMBETTES, P. L., AND PESQUET, J.-C. *Fixed-Point Algorithms for Inverse Problems in Science and Engineering*. Springer New York, New York, NY, 2011, ch. Proximal Splitting Methods in Signal Processing, pp. 185–212.
- [25] COMBETTES, P. L., AND PESQUET, J.-C. Stochastic approximations and perturbations in forward-backward splitting for monotone operators. *Pure and Applied Functional Analysis* 1, 1 (2016), 13–37.
- [26] DE PIERRO, A. R., AND YAMAGISHI, M. E. B. Fast EM-like methods for maximum “a posteriori” estimates in emission tomography. *Medical Imaging, IEEE Transactions on* 20, 4 (2001), 280–288.
- [27] DEM’YANOV, V. F., AND VASIL’EV, L. V. *Nondifferentiable optimization*. Springer, 1985.
- [28] DEWARAJA, Y. K., KORAL, K. F., AND FESSLER, J. A. Regularized reconstruction in quantitative SPECT using CT side information from hybrid imaging. *Physics in Medicine and Biology* 55, 9 (2010), 2523.
- [29] HARMANY, Z. T., MARCIA, R. F., AND WILLETT, R. M. This is SPIRAL-TAP: Sparse Poisson Intensity Reconstruction Algorithms - theory and practice. *IEEE Transactions on Image Processing* 21, 3 (2012), 1084–1096.
- [30] HELOU, E. S., CENSOR, Y., CHEN, T.-B., CHERN, I.-L., DE PIERRO, Á. R., JIANG, M., AND LU, H. H.-S. String-averaging expectation-maximization for maximum likelihood estimation in emission tomography. *Inverse Problems* 30, 5 (2014), 055003.
- [31] HERMAN, G. T. *Fundamentals of computerized tomography: image reconstruction from projections*. Advances in Computer Vision and Pattern Recognition. Springer-Verlag London, 2009.
- [32] HIRIART-URRUTY, J.-B., AND LEMARÉCHAL, C. *Convex Analysis and Minimization Algorithms I and II*. A Series of Comprehensive Studies in Mathematics. Springer-Verlag, Berlin, 1993.
- [33] HOFFMANN, A. The distance to the intersection of two convex sets expressed by the distances to each of them. *Mathematische Nachrichten* 157, 1 (1992), 81–98.
- [34] HUDSON, H. M., AND LARKIN, R. S. Accelerated image reconstruction using ordered subsets of projection data. *Medical Imaging, IEEE Transactions on* 13, 4 (1994), 601–609.

- [35] JOHANSSON, B., RABI, M., AND JOHANSSON, M. A randomized incremental subgradient method for distributed optimization in networked systems. *SIAM Journal on Optimization* 20, 3 (2010), 1157–1170.
- [36] KAK, A. C., AND SLANEY, M. *Principles of Computerized Tomographic Imaging*. IEEE press, 1988.
- [37] KIBARDIN, V. M. Decomposition into functions in the minimization problem. *Avtomatika i Telemekhanika*, 9 (1979), 66–79.
- [38] NATTERER, F. *The Mathematics of Computerized Tomography*. Wiley, 1986.
- [39] NATTERER, F., AND WÜBBELING, F. *Mathematical methods in image reconstruction*. SIAM, 2001.
- [40] NEDIĆ, A., AND BERTSEKAS, D. P. Incremental subgradient methods for nondifferentiable optimization. *SIAM Journal on Optimization* 12, 1 (2001), 109–138.
- [41] NETO, E. S. H., AND DE PIERRO, A. R. Convergence results for scaled gradient algorithms in positron emission tomography. *Inverse problems* 21 (2005), 1905.
- [42] NETO, E. S. H., AND DE PIERRO, Á. R. Incremental subgradients for constrained convex optimization: a unified framework and new methods. *SIAM Journal on Optimization* 20, 3 (2009), 1547–1572.
- [43] PENFOLD, S. N., SCHULTE, R. W., CENSOR, Y., BASHKIROV, V., McALLISTER, S., SCHUBERT, K. E., AND ROSENFELD, A. B. Block-iterative and string-averaging projection algorithms in proton computed tomography image reconstruction. *Biomedical Mathematics: Promising Directions in Imaging, Therapy Planning and Inverse Problems* (2010), 347–367.
- [44] POLYAK, B. T. Introduction to optimization. 1987. *Optimization Software, Inc, New York*.
- [45] RAGUET, H., FADILI, J., AND PEYRÉ, G. A generalized forward-backward splitting. *SIAM Journal on Imaging Sciences* 6, 3 (2013), 1199–1226.
- [46] SHEPP, L. A., AND VARDI, Y. Maximum likelihood reconstruction for emission tomography. *Medical Imaging, IEEE Transactions on* 1, 2 (1982), 113–122.
- [47] SHOR, N. Z. *Minimization methods for non-differentiable functions*. Springer-Verlag New York, Inc., 1985.
- [48] SOLODOV, M. V. Incremental gradient algorithms with stepsizes bounded away from zero. *Computational Optimization and Applications* 11, 1 (1998), 23–35.
- [49] SOLODOV, M. V., AND ZAVRIEV, S. K. Error stability properties of generalized gradient-type algorithms. *Journal of Optimization Theory and Applications* 98, 3 (1998), 663–680.
- [50] SUNDHAR RAM, S., NEDIĆ, A., AND VEERAVALLI, V. V. Incremental stochastic subgradient algorithms for convex optimization. *SIAM Journal on Optimization* 20, 2 (2009), 691–717.

- [51] SUNDHAR RAM, S., NEDIĆ, A., AND VEERAVALLI, V. V. Distributed stochastic subgradient projection algorithms for convex optimization. *Journal of optimization theory and applications* 147, 3 (2010), 516–545.
- [52] TANAKA, E., AND KUDO, H. Subset-dependent relaxation in block-iterative algorithms for image reconstruction in emission tomography. *Physics in medicine and biology* 48, 10 (2003), 1405.
- [53] TSENG, P. An incremental gradient (-projection) method with momentum term and adaptive stepsize rule. *SIAM Journal on Optimization* 8, 2 (1998), 506–531.
- [54] VARDI, Y., SHEPP, L., AND KAUFMAN, L. A statistical model for positron emission tomography. *Journal of the American Statistical Association* 80, 389 (1985), 8–20.
- [55] YAMADA, I., AND OGURA, N. Adaptive projected subgradient method for asymptotic minimization of sequence of nonnegative convex functions. *Numerical Functional Analysis and Optimization* 25, 7 (2005), 593–617.
- [56] YAMADA, I., AND OGURA, N. Hybrid steepest descent method for variational inequality problem over the fixed point set of certain quasi-nonexpansive mappings. *Numerical Functional Analysis and Optimization* 25, 7 (2005), 619–655.